X-Ray Telescopes

Marco Barbera

Dipartimento di Scienze Fisiche ed Astronomiche
Università degli Studi di Palermo

Outline

- Basic principles of X-ray focusing
- Main Telescopes Characteristics
- Telescope Geometries
- Manufacturing Technologies

Some milestones in X-ray Optics for Astrophysics

- **1948:** First successful attempt to focus an X-ray beam by a total-reflection optics (Baez)
- **1952:** H**.** Wolter proposes to use two-reflection optics based on conics for X-ray microscopy
- **1960:** R. Giacconi and B. Rossi propose to use grazing incidence optics for X-ray telescopes
- **1963:** Giacconi and Rossi fly the **first (small) X-ray telescope to take images of the Sun**
- **1973: SKYLAB** carries onboard two small X-ray optics to take images of the solar corona
- **1978: Einstein**, the **first satellite with focusing optics entirely dedicated to X-rays**
- **1983: EXOSAT** first European mission with X-ray optics on board
- **1990: ROSAT**, **first X-Ray All Sky Survey with a high resolution focusing telescope**
- **1993: ASCA**, a multimodular X-ray telescope with high effective area for high res. spectroscopy
- **1996: BeppoSAX**, a broad-band satellite with on-board a Ni electroformed replicated optics
- **1999: Chandra,** an X-ray telescope with **sub-arcsec angular resolution**
- **1999: XMM-Newton**, an X-ray telescope (3 mirror modules) with **EA > 4000 cm^2 @ 1 keV**
- **2005: Suzaku,** high throughput thin foil X-ray optics for high res. spectroscopy with bolometers

Why focusing X-rays with telescopes

1. To obtain imaging capability (angular resolution and morphology)

2. To Increase the collecting area, reduce the detector BKG and thus reduce the source detection limit

Direct Vision Detectors

$$I_{min}(E) = \frac{n_\sigma}{QE}\sqrt{\frac{B(E)}{A_D \cdot \Delta t \cdot \Delta E}}$$

Focusing Telescopes

$$I_{min}(E) = \frac{n_\sigma}{QE \cdot A_{eff}(E)}\sqrt{\frac{B(E) \cdot A_{SD}}{\Delta t \cdot \Delta E}}$$

$I_{min}(E)$ = Src. Det. Limit [cts/(s·cm^2·keV)]

$B(E)$ = Detector BKG [cts/(s·cm^2·keV)]

A_D = Detector Collecting Area [cm^2]

n_σ = statistical significance

QE = Detector Quantum Efficiency

Δt = Integration Time [s]

A_{SD} = Src. Collecting Area [cm^2]

$A_{eff}(E)$ = Telescope Eff. Area [cm^2]

3. To concentrate the source into a small area and allow the use of high energy resolution dispersive spectrometer.

Basic Principles of X-Ray Focusing

Plane Wave Propagation

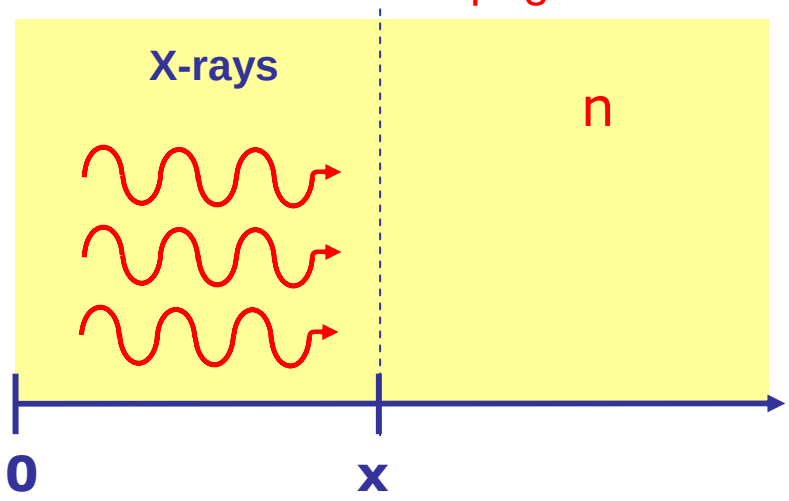

$$E(x,t) = E_0 e^{i\omega(\frac{n \cdot x}{c} - t)}$$

Refraction Index

$n = 1 - \delta + i\beta$

$$E(x,t) = E_0 \cdot \underbrace{e^{i\omega(\frac{x}{c} - t)}}_{\text{Propagation}} \underbrace{e^{-i(\frac{\omega\delta \cdot x}{c})}}_{\text{Phase shift}} \underbrace{e^{-\frac{\omega\beta \cdot x}{c}}}_{\text{Absorption}}$$

The real part $(1 - \delta)$ of the refractive index of a material is slightly less than 1 in the energy range of X-rays with typical values of $\delta < 10^{-4}$.

X-Ray Interaction with Matter

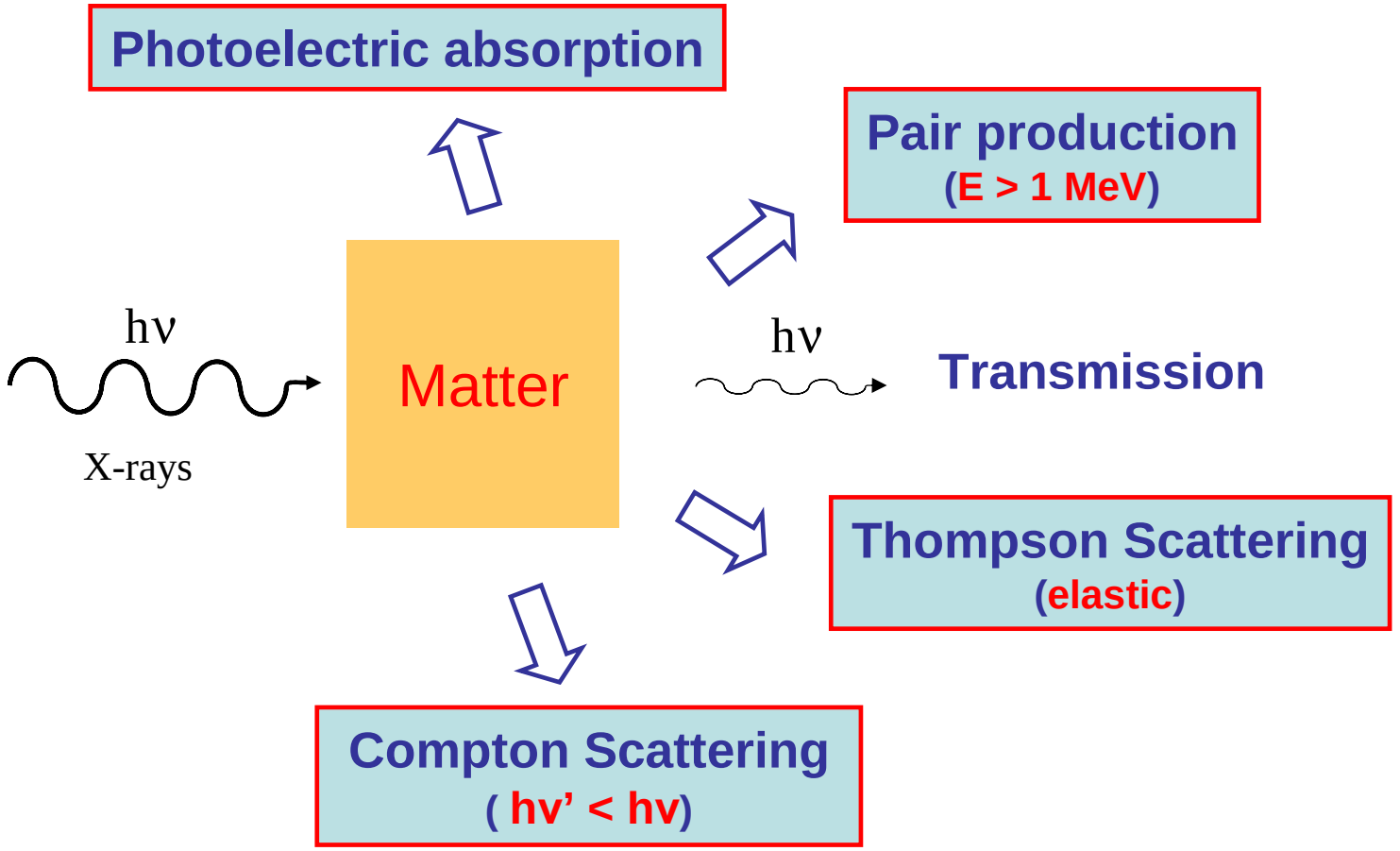

At X-ray energies lower than about 50 keV (except for very light elements) the atomic cross-section is largely dominated by the photoelectric absorption.

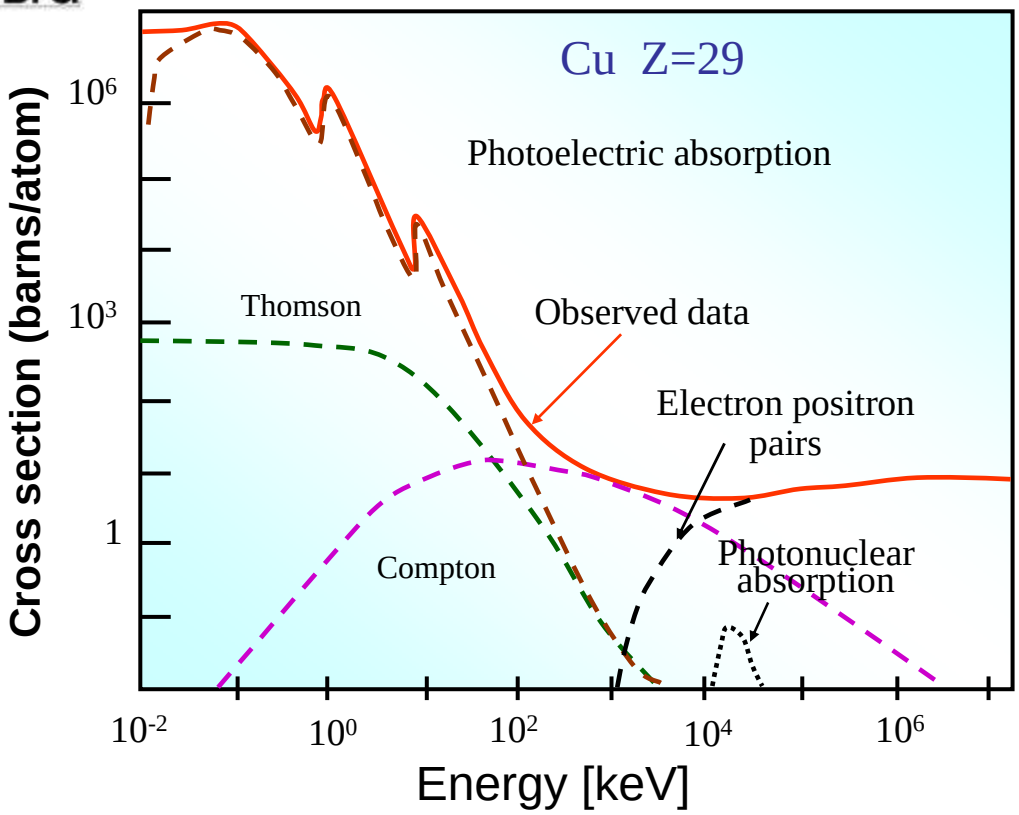

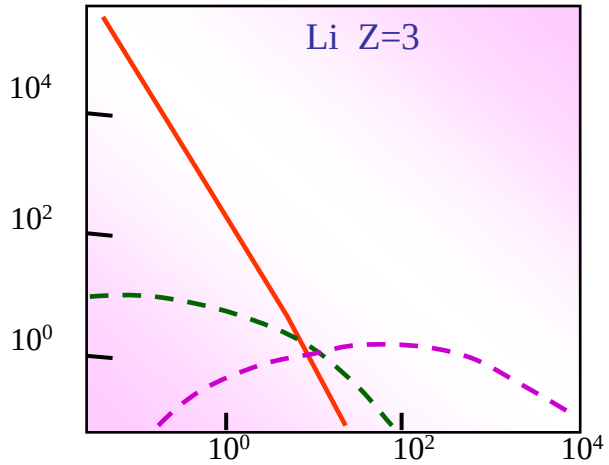

1 Barn = 10^{-28} [m^2]

$$\delta = \frac{1}{2\pi}\frac{e^2}{m_e c^2}\frac{N_0\rho}{A}\lambda^2 f_1$$

$$\beta = \frac{1}{2\pi}\frac{e^2}{m_e c^2}\frac{N_0\rho}{A}\lambda^2 f_2$$

Well above an absorption edge, $f_1 \sim N_e$ (number of electrons with binding energy lower than the edge).

Total External Reflection

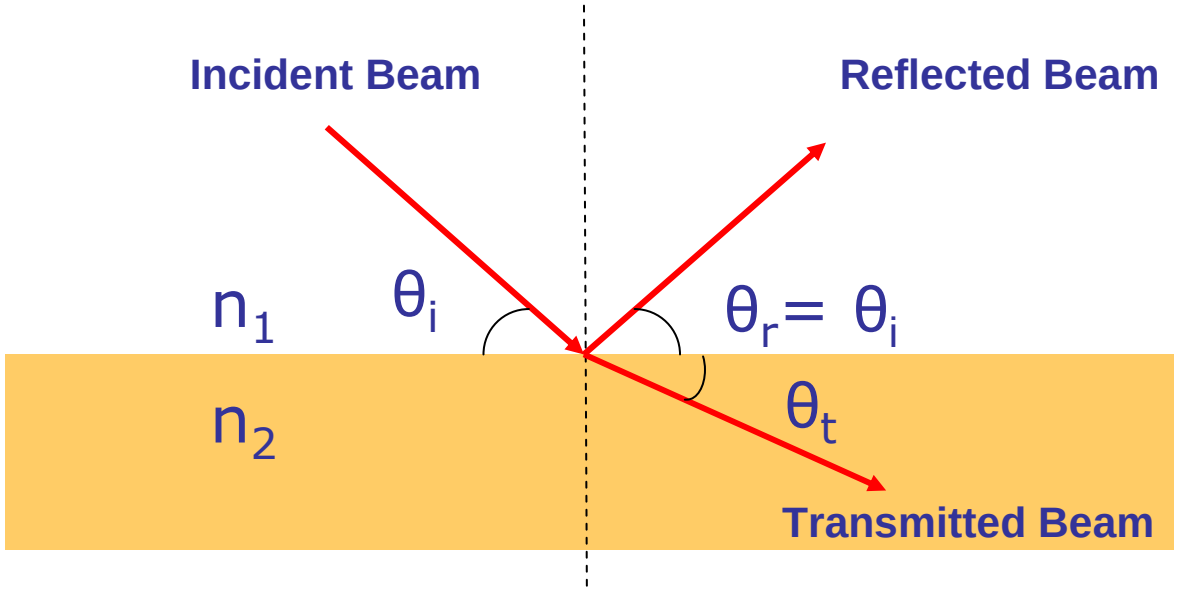

According to Snell law

$$n_1 \cos\theta_i = n_2 \cos\theta_t$$

If $n_1 > n_2$ there is a value of the incident angle θ_i (critical angle) such that the angle of the transmitted beam $\theta_t = 0$ and the beam is totally reflected.

$$\cos\theta_i = \frac{n_2}{n_1}$$

If the first medium is vacuum ($n_1 = 1$) than the critical value of the incident angle is

$$\cos\theta_{crit} = n_2$$

In the small angle approximation ($\theta < 15^\circ$) and using the expression for the real part of the refraction index $n = 1 - \delta$ we have

$$\cos\theta_{crit} \approx 1 - \frac{\theta_{crit}^2}{2} \approx 1 - \delta$$

$$\theta_{crit} \approx \sqrt{2\delta}$$

As previously mentioned, at energies above an absorption edge, f1 ~ Ne (number of electrons with binding energy lower than the edge) and thus we can write $f_1 \propto Z$ and thus

$$\delta \propto \frac{Z}{E^2}$$

$$\theta_c \propto \frac{\sqrt{Z}}{E}$$

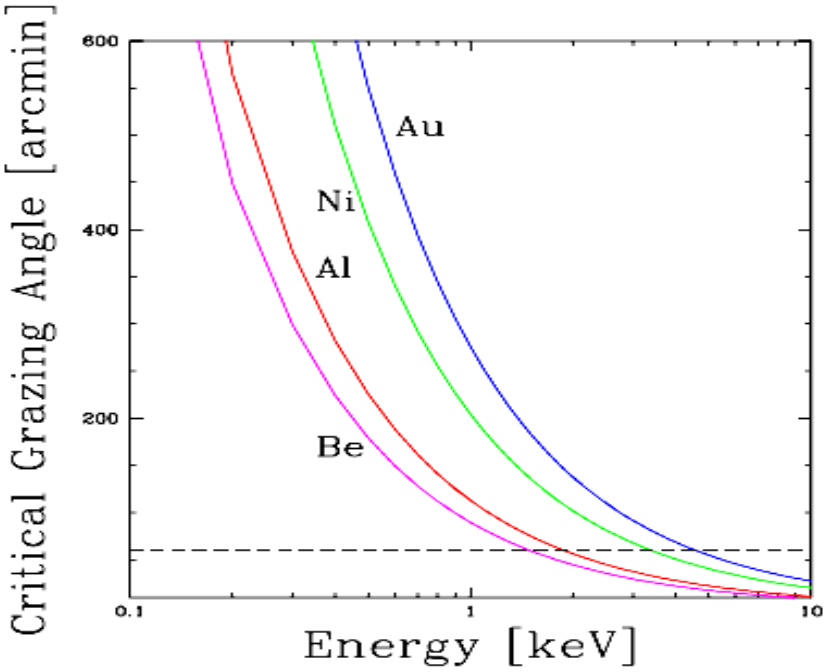

$$\theta_c \propto \frac{\sqrt{Z}}{E}$$

Higher Z materials reflect at a given energy with larger incidence angles.

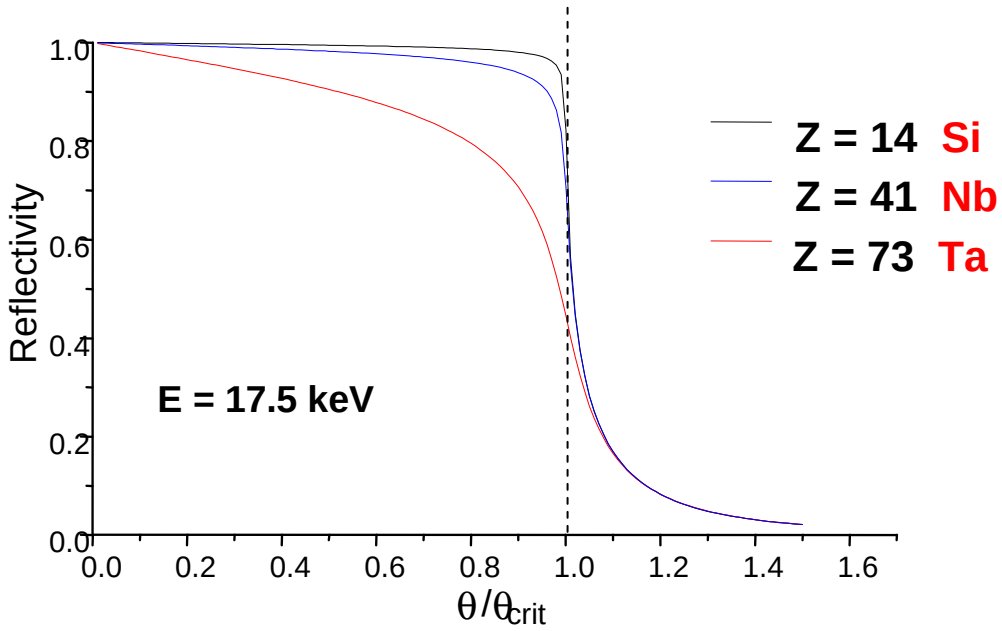

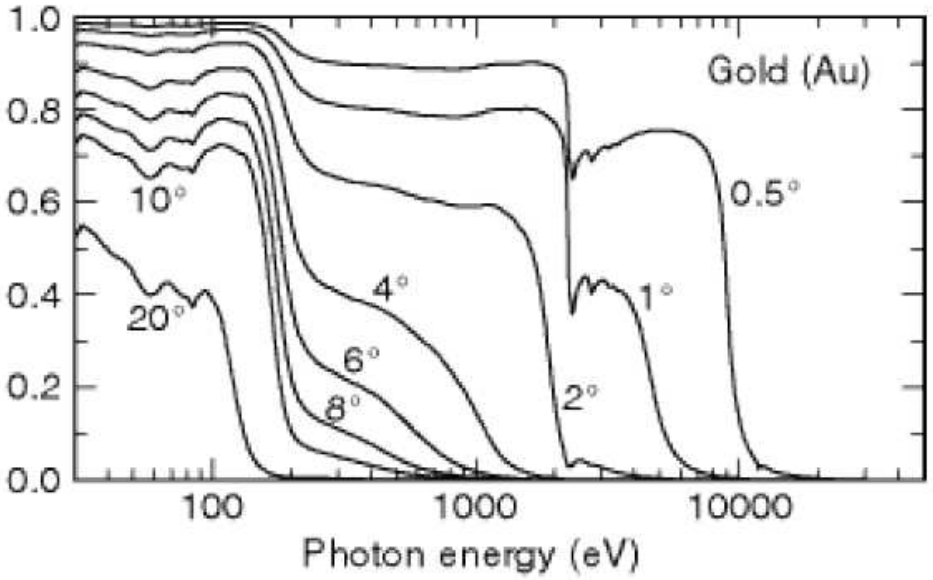
Gold (Au)
10°
20°
4°
6°
8°
2°
1°
0.5°
1.0
0.8
0.6
0.4
0.2
0.0
100
1000
10000
Photon energy (eV)

X-Rays

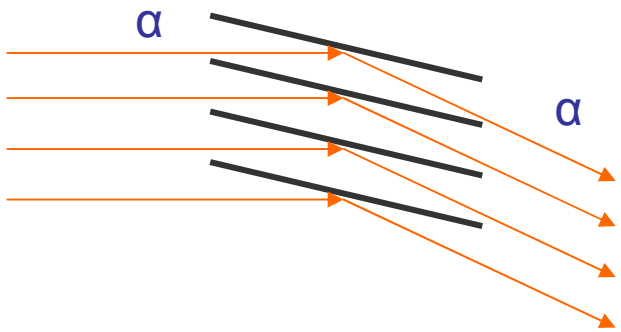
α
α

α ~ 1°

How to focus X-rays at E > 10 keV

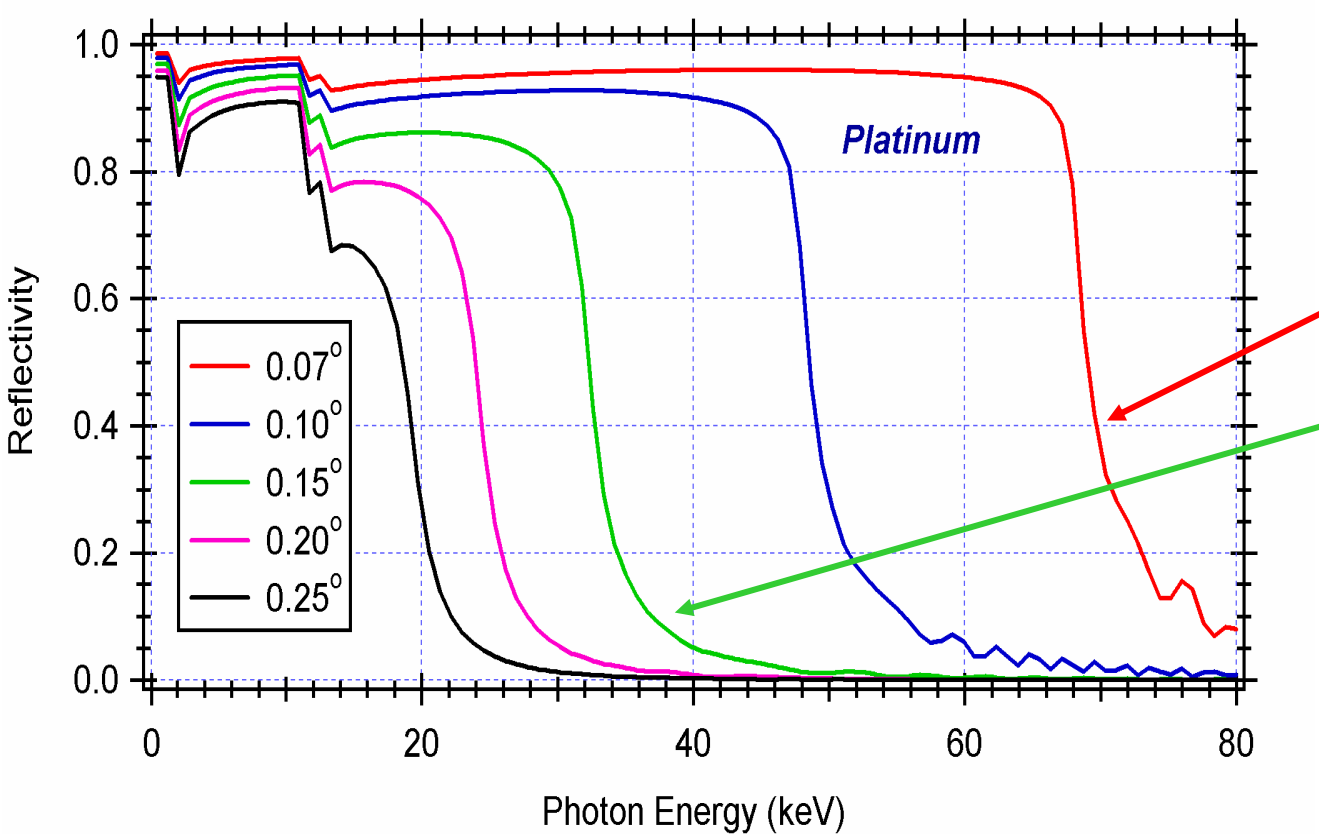

Two reflections

F.L. = R · tg (4α)

F.L. ~ 100 m

F.L. ~ 50 m

$$E \propto \frac{\sqrt{Z}}{\theta_c}$$

X-ray telescopes based on total reflection are not practical for X-rays > 10 keV.

Focusing by Bragg Diffraction (reflection)

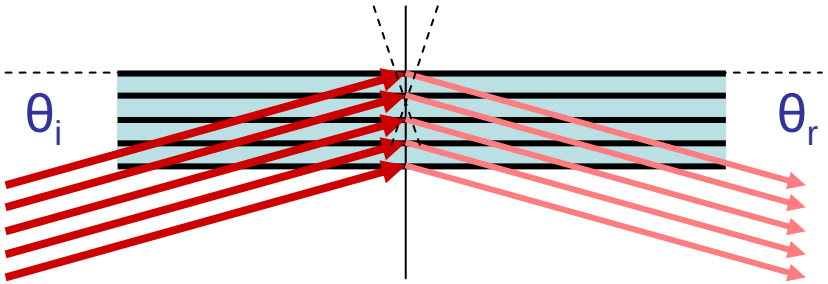

Constructive Interference for the reflected beam when Bragg Law is satisfied

$$2d \sin\theta = n\lambda$$

A constant period multilayer structure behaves like a natural crystal with crystal planes parallel to the reflecting surface, and provides increased reflection efficiency in a narrow band.

Two materials, one with low Z (e.g. Si, C), and one with high Z (e.g. W, Ni, Mo) are deposited in sequence on a substrate.

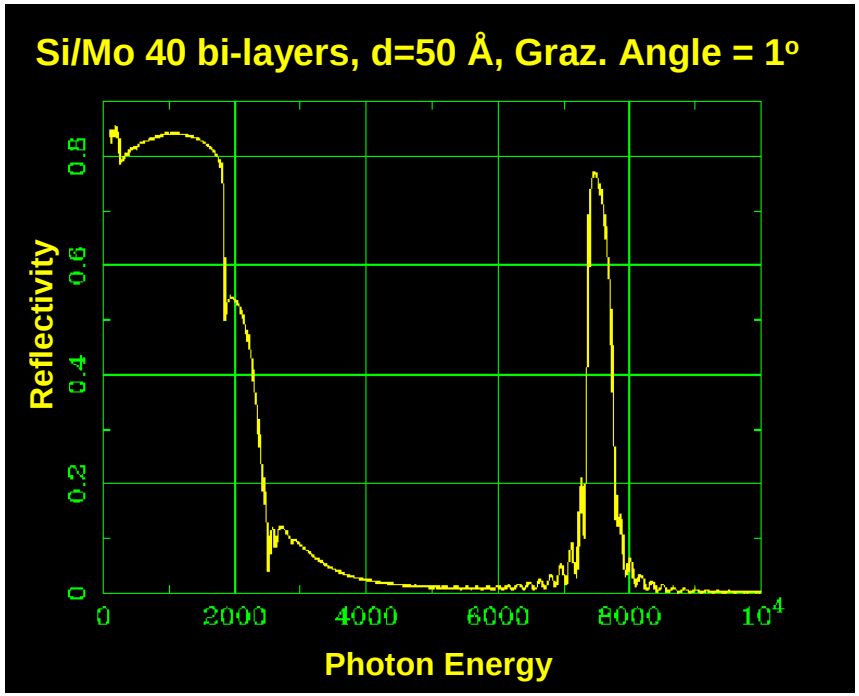

The period of the multi-layer structure D is the thickness of one bi-layer. Typical values of D range between 20 and 200 Å.

A number of by-layer ranging between a few tens to a few hundreds are usually deposited to obtain an optimal gain in reflectivity.

At each interface, due to scattering by rough surfaces, the reflectivity is reduced by a factor nearly

$$e^{-\left(\frac{2\pi\cdot\sigma}{D}\right)}$$

An RMS surface roughness σ < D/10 would be ideally required.

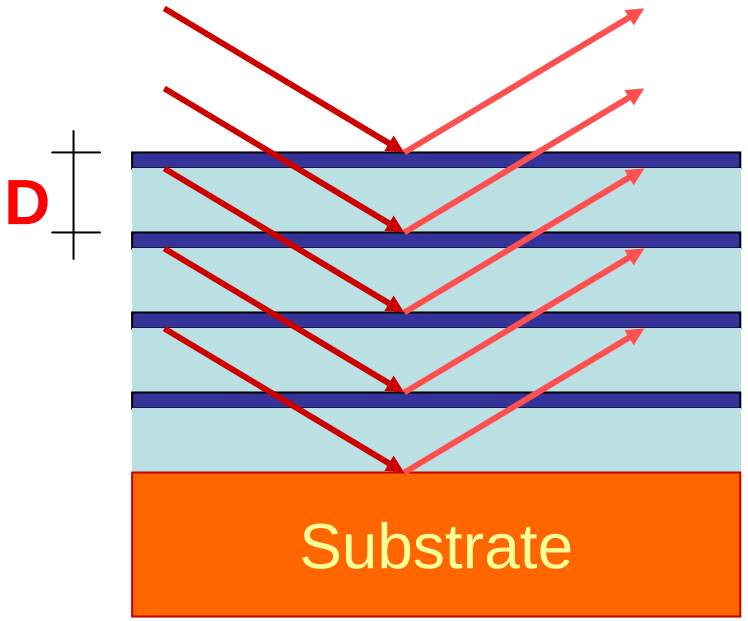

Graded Multilayers

If the D spacing of the multilayer is not constant, different wavelengths satisfy the Bragg law and the reflectivity can be increased over a wide energy band.

The D spacing of the i_{th} bi-layer follows a recipe such as $D(i) = a \cdot (b+i)^{-c}$ with the constraints that $D(1) = D_{MAX}$, and $D(N) = D_{MIN}$

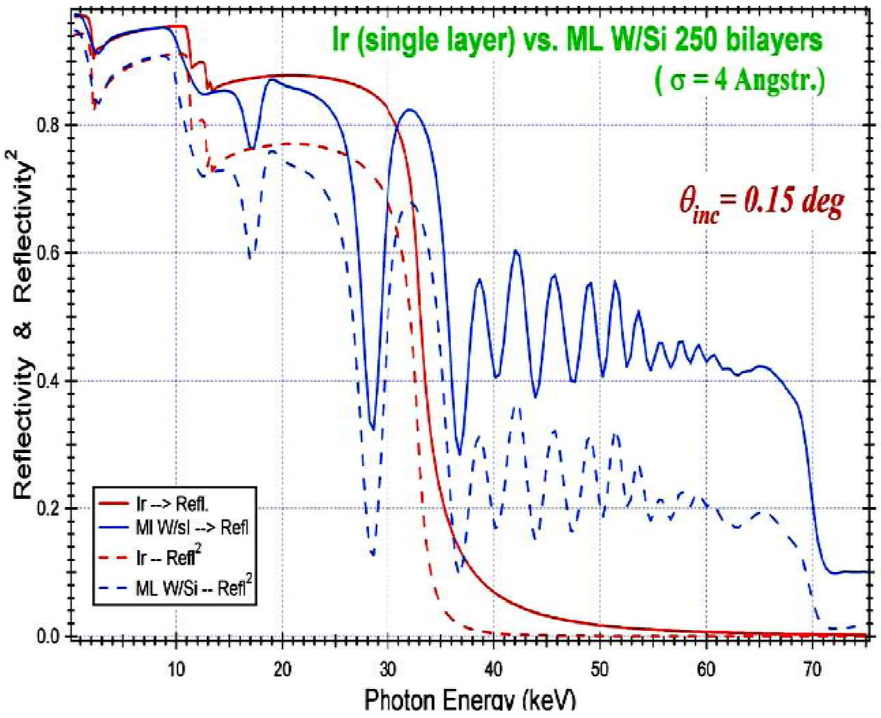

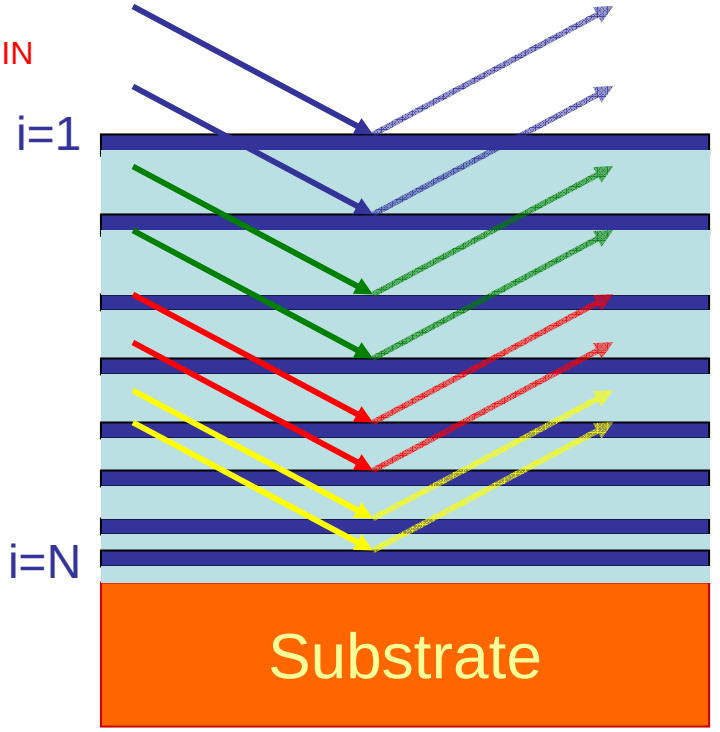

Focusing X-Rays by Coded Masks

A pattern of open and blocked pixels on a thick mask produces a patterned image of a point source on the imaging detector.

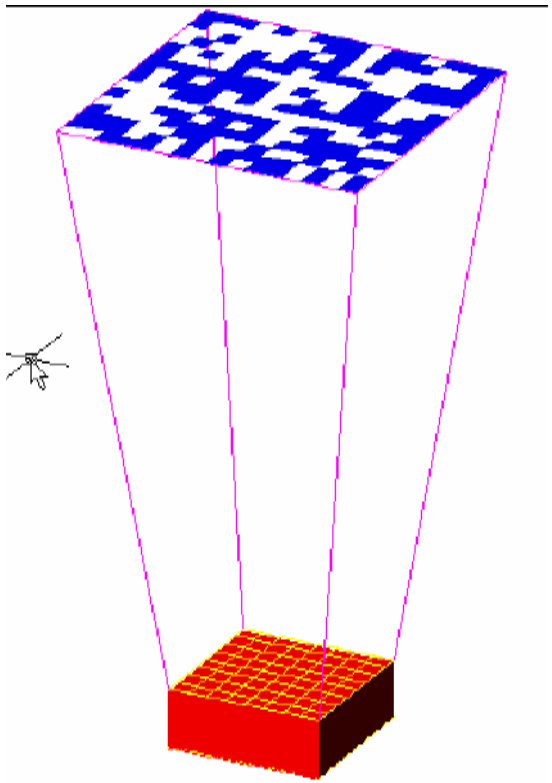

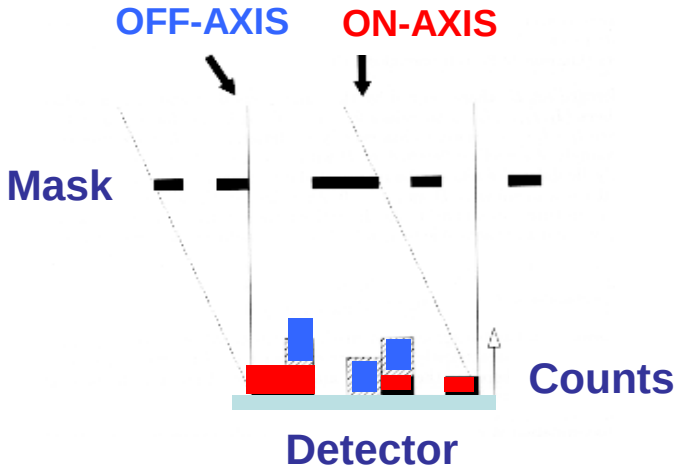

The detected pattern is a convolution of the Source and the Mask Pattern plus the detector Background. $D = S \otimes M + B$

The pattern produced by a point source fully illuminates the detector thus source detection is strongly affected by the detector background.

Focusing X-Rays by Laue Diffraction (transmission)

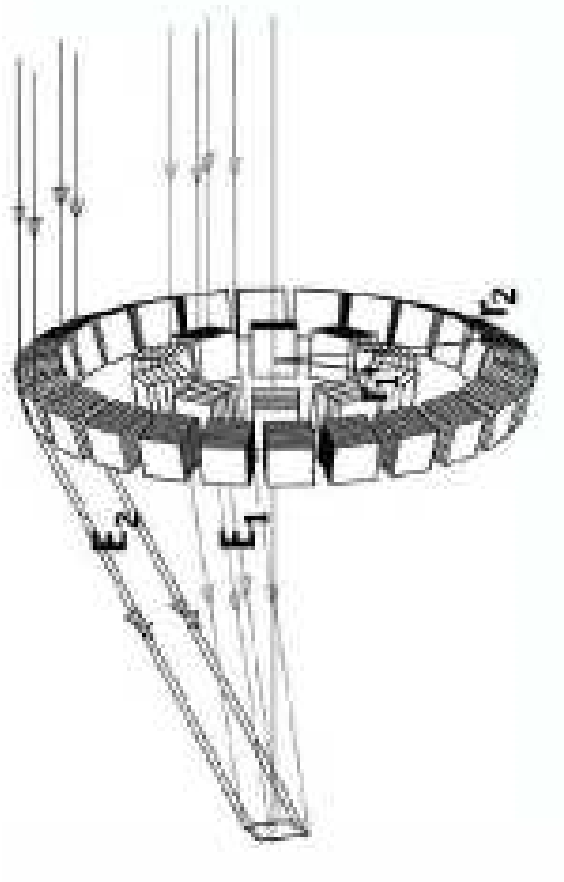

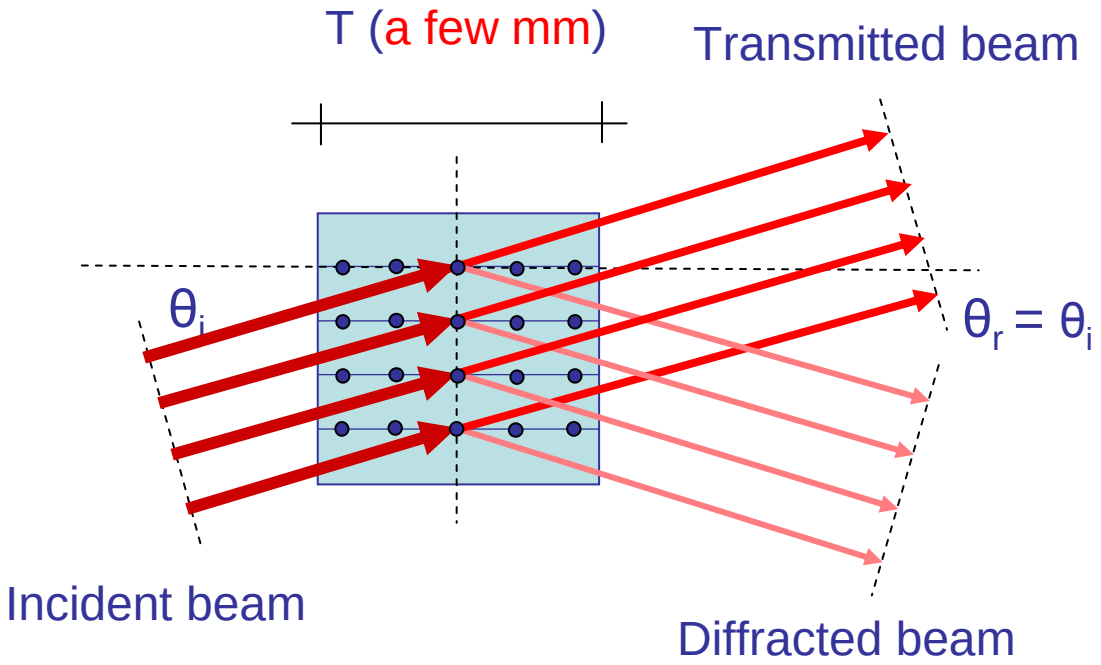

Constructive Interference (in transmission) for a given crystal plane orientation when Bragg Law is satisfied

$$2d \sin\theta = n\lambda$$

- Small Reflection Efficiency (< 10 %)

The reflection efficiency is a function of the thickness of the crystal T, the absorption coefficient μ, and the secondary extinction coefficient σ (probability per unit length that X-ray photons are diffracted).

$$R(E) = \frac{I_D}{I_o} \approx \frac{1}{2}(1 - e^{-2\sigma T}) \cdot e^{-\mu \frac{T}{\cos\theta}}$$

- Monochromatic

The use of mosaic crystals and proper geometry of the Laue Lense to include a range of angle of incidence allows for an increase of the band-pass.

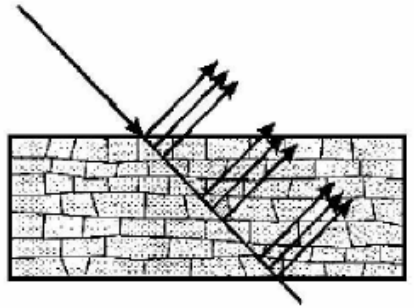

- Pointing accuracy and off-axis strongly affect energy responce

Main Telescope Characteristics

EFFECTIVE AREA. Geometric collecting area multiplied by the reflection efficiency. It is partially affected by masking of the reflecting surfaces by mechanical mounting structures.

The EA of X-ray telescopes, usually expressed in cm^2, is a funcion of energy and off-axis angle.

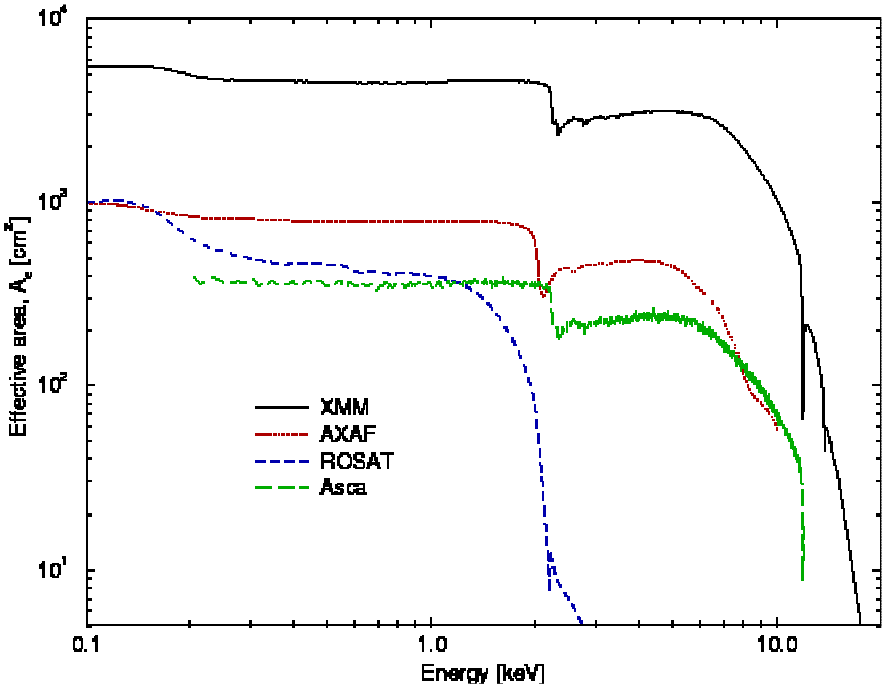

Effective Area vs. energy for the XMM-Newton, Chandra, ROSAT and ASCA Mirror Assemblies.

The reduction of the illumination of the full geometric area of the telescope moving from on-axis towards the border of the FOV is called Vignetting.

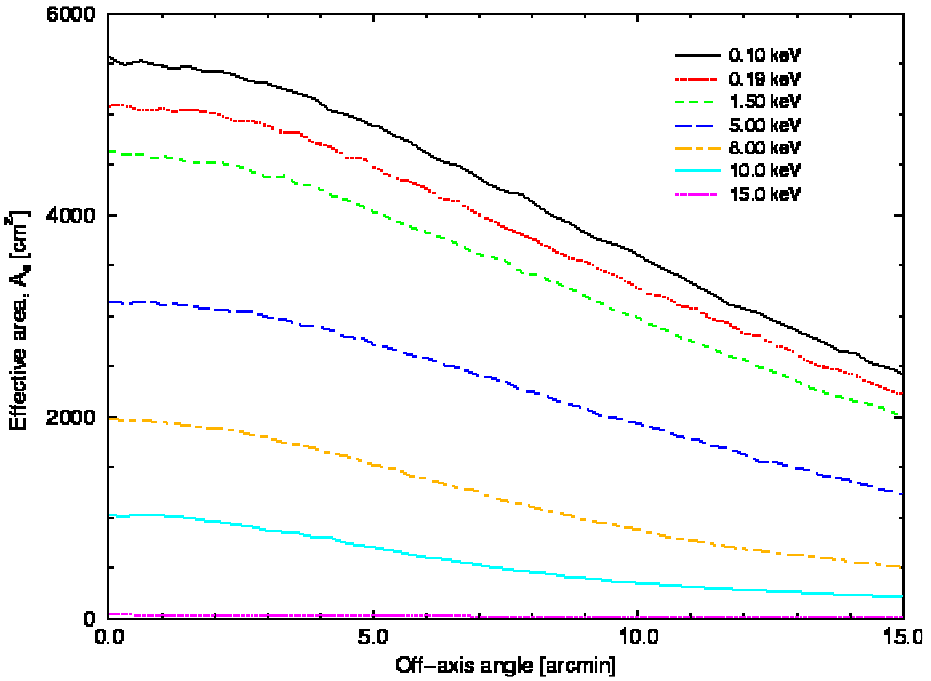

Effective Area vs. Off-axis angle at different energies for the XMM-Newton Mirror Assembly

ANGULAR RESOLUTION. Minimum angular distance between two point sources that are well separated at the focal plane. The AR of X-ray telescopes depends on the off-axis angle and only moderately on energy. The AR is usually expressed in arcsec or arcmin.

The AR is usually defined as the width of the image of a point source (Point Spread Function).

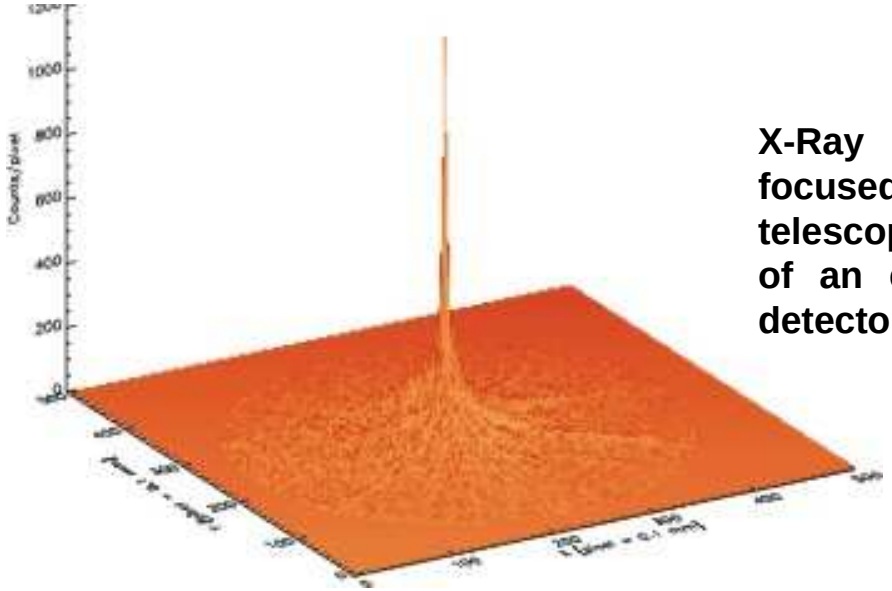

X-Ray Image of a Point Source (PSF) focused by a grazing incidence X-Ray telescope with cylindrical geometry (approx. of an ellipse) onto a Microchannel Plate detector.

Two parameters are used to characterize this width: the Full Width at Half Maximum (FWHM) and the Half Energy Width (HEW).

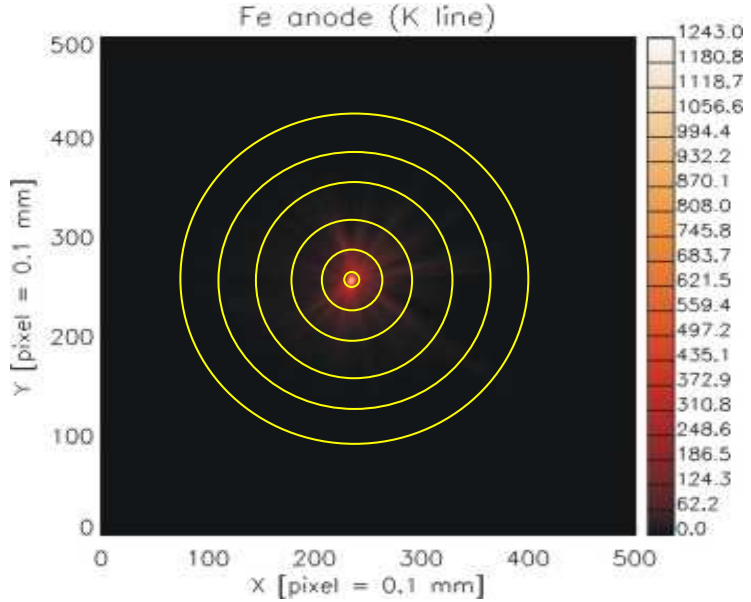

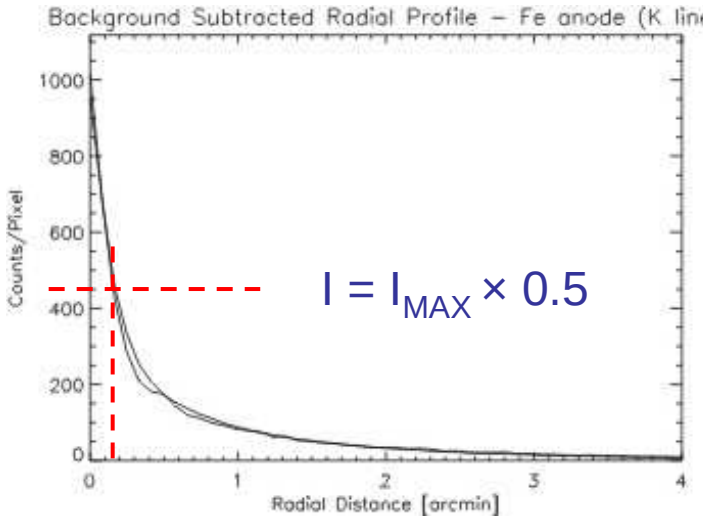

FWHM = 2 × 0.15 arcmin

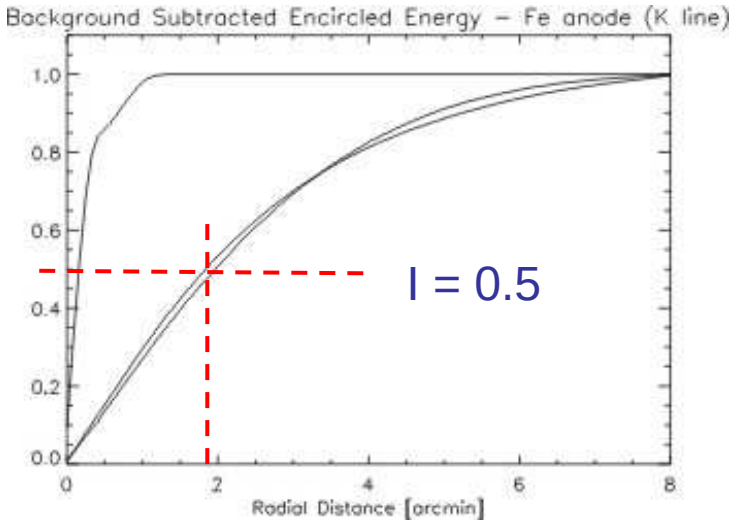

HEW = 2 × 1.8 arcmin

Limiting factors for the Angular Resolution

- **Diffraction**
- **Optical Aberrations**
  - Spherical Aberration
  - Coma
  - Astigmatism
- **Surface Quality Errors**
- **Figure Errors**

DIFFRACTION LIMIT. A monochromatic plane wave passing through a circular aperture produces a diffraction pattern.

The central peak of the diffraction pattern (Airy Disk) has an angular radius

$$\theta = 1.22 \cdot \lambda/D$$

where D is the diameter of the aperture.

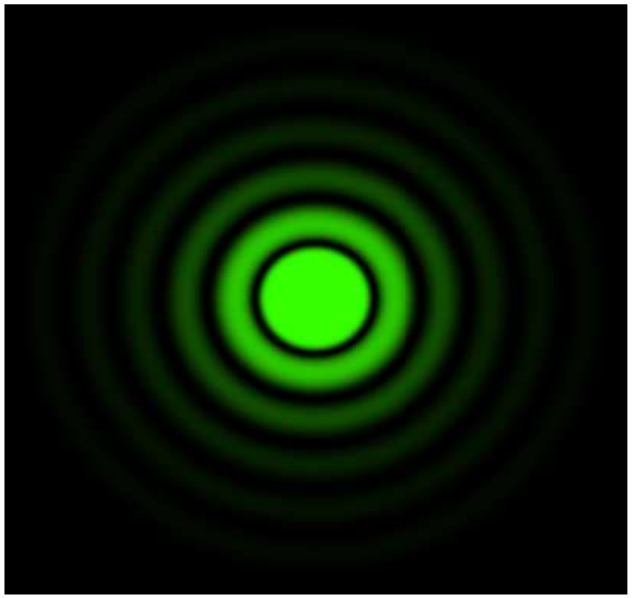

$$\Delta\theta = 1.22\ \lambda/D$$

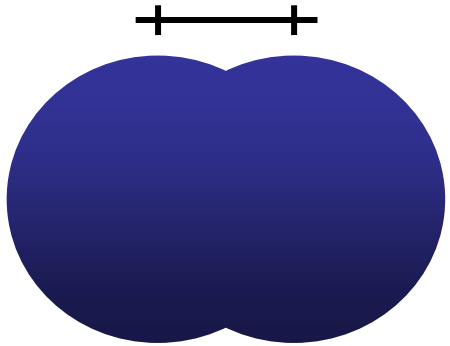

Diffraction Limit of a Telescope

SPHERICAL ABERRATION. Parallel rays hitting the optics close to the optical axis (paraxial rays) are focused further away with respect to marginal rays. The overall effect is a blurring of the focal spot. Only the parabola is completely un-affected by this aberration.

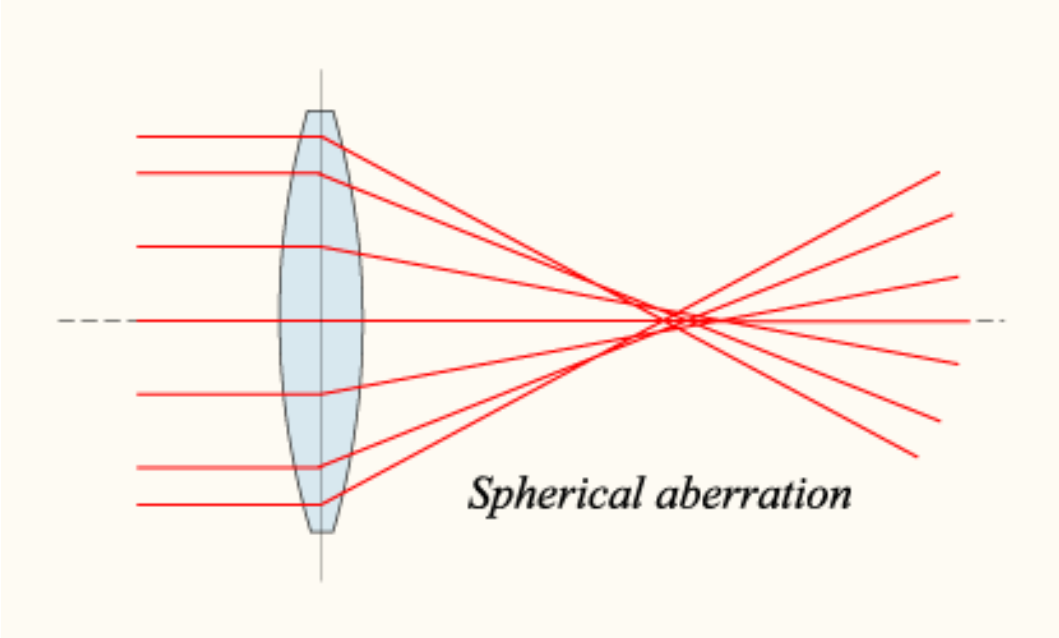

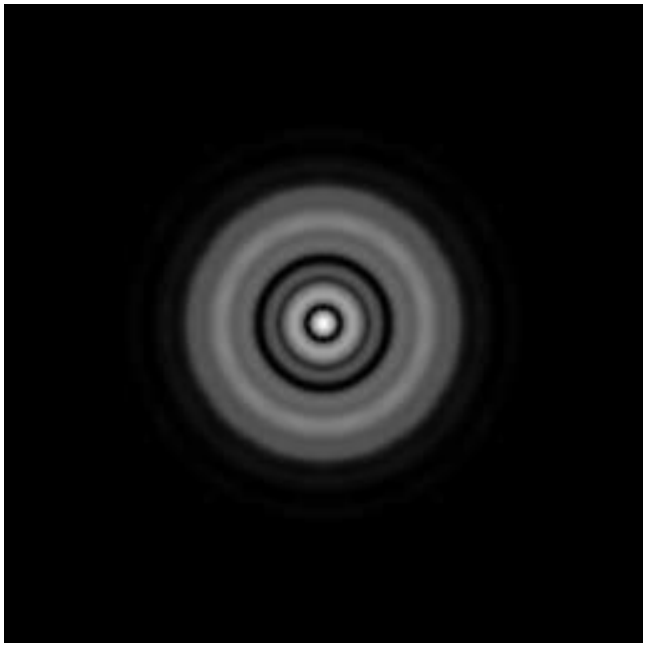

ASTIGMATISM – This aberration comes from misallignement of different optical elements fo the telescope or different curvature of an element as a function of the azimuthal angle. The focal spot of an optical system suffering from astigmatism is usually elliptical.

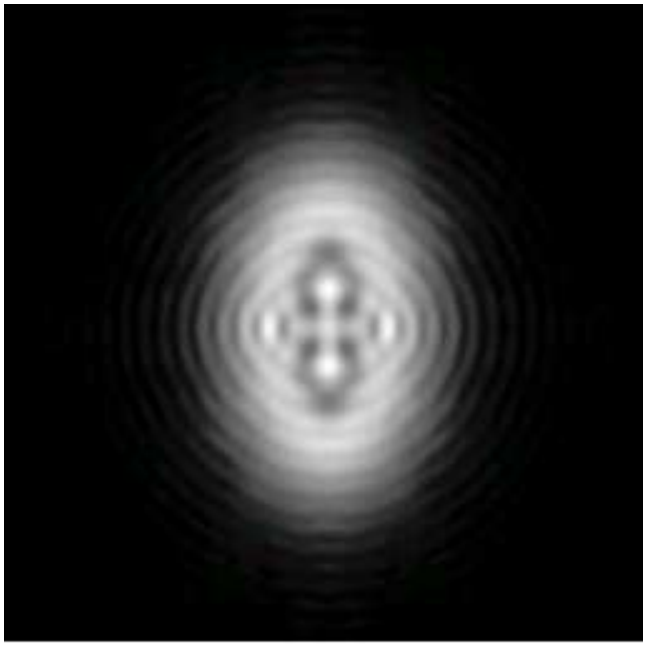

COMA – Is an aberration similar to the spherical one, but for off-axis angle parallel beams. Different rings on the telescope form focal spots ad different focal distances and different off-axis positions. The resulting image from the superposition of the various contribution has a typical shape of a bright spot followed by a large tail like a Comet. The coma aberration is particularly pronounced in reflecting telescopes especially at the border of the FOV.

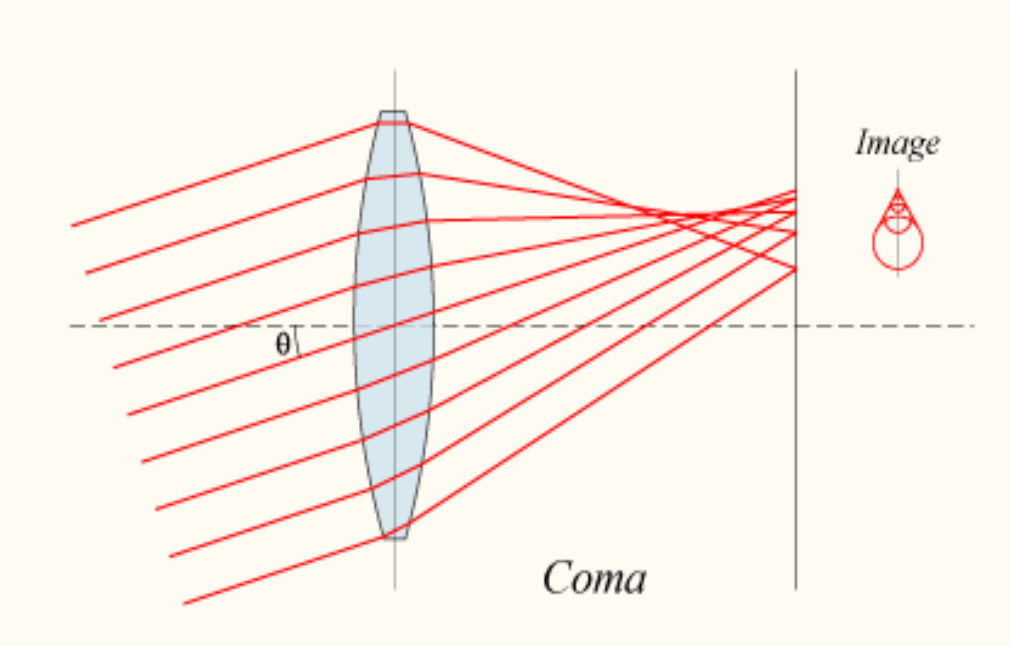

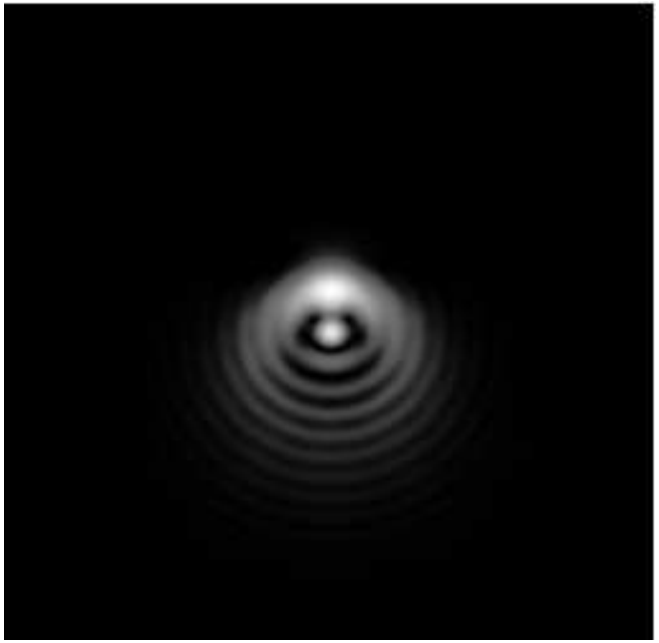

SURFACE QUALITY ERRORS. If a reflecting telescope has a high surface roughness a fraction of the incoming radiation can be scattered deteriorating the angular resolution and eventually reducing the effective area.

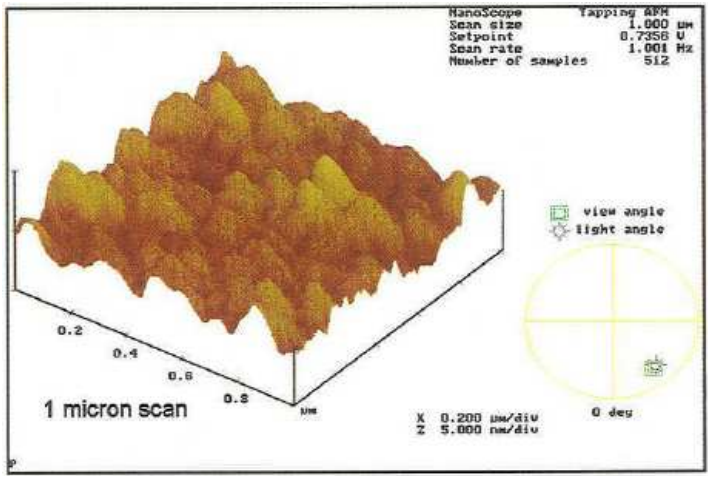

First order scattering theory gives the total integrated scatter (TIS) of X-rays of wavelength λ, at grazing angle θ_g on a reflecting surface as

$$TIS \approx 4\pi \cdot \left(\frac{\sigma \cdot \sin \vartheta_g}{\lambda} \right)^2$$

where σ is the rms surface roughness.

$$\sigma^2 = \frac{1}{L} \int_0^L h(x)^2 \cdot dx$$

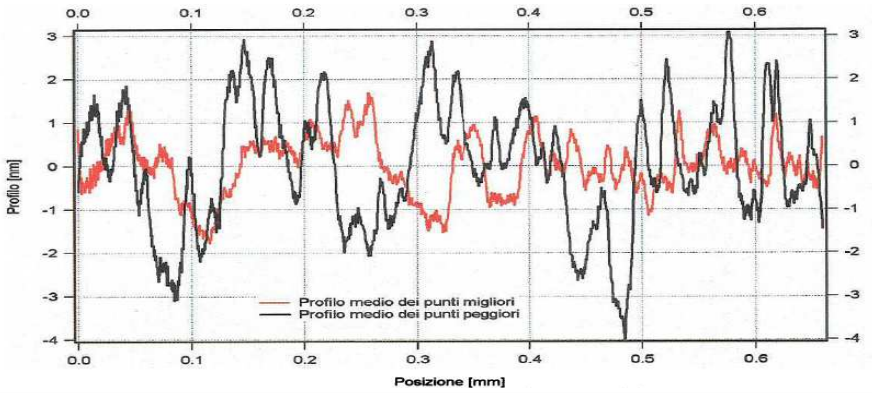

At a grazing angle of 1° and energy of 1 keV (λ = 12.4 Å), in order to get a fraction of scattered light lower than 10% the surface roughness has to be σ < 60 Å. At 10 keV the surface roughness should be ten times better.

The surface quality of reflecting telescopes for E > 10 keV is one of the major technical difficulties for the construction of such focusing systems.

FIGURE AND MOUNTING ERRORS – Deformations from the ideal geometry can be introduced during the construction, assembling or operation of the various optical elements of the telescope.

Such errors dominate the angular resolution in many of the construction technologies currently used for X-Ray telescopes.

Is X-Ray Astronomy Diffraction Limited ?

If we consider an X-Ray telescope ($\lambda < 100$ Å) with a diameter $D = 1$ m, the calculated diffraction limit is

$$\Delta\theta = 1.22\ \lambda/D < 0.002 \text{ arcsec}$$

The aberrations previously discussed significantly deteriorate the imaging capability of the X-Ray telescopes built up to now. The best angular resolution measured up to now has been obtained with the Chandra X-ray telescope and is of the order of 0.5 arcsec FWHM on-axis.

X-Ray Telescopes for Astrophysics are currently far from being diffraction limited.

Geometries of X-Ray Focusing Optics

Kirkpatrick-Baez two crossed reflections

Kirkpatrick and Baez in 1948 proposed the first practical system to make X-ray images. The K-B optical system consists of two crossed parabolas or ellipses of translation (Figure A). More shells can be nested to increase the effective area (Figure B).

The K-B is easy to make since each element is obtained by thermally or mechanically bending of a flat surface.

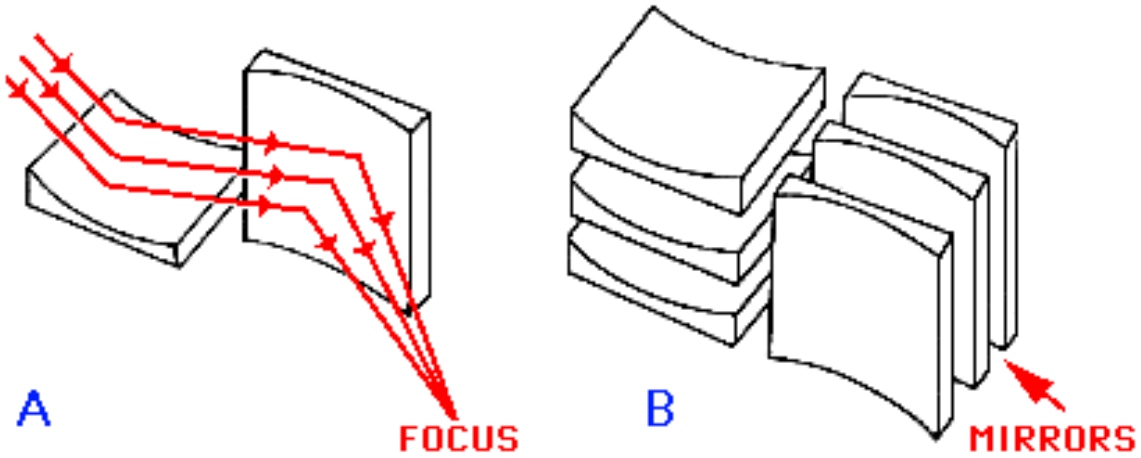

The K-B strongly affected by Coma abberration and thus has a narrow FOV useful for sharp imaging.

Paraboloid

In 1960 Giacconi and Rossi proposed to use an imaging telescope to focus solar and cosmic X-rays. They also proposed to nest multiple confocal shells to increase the collecting area. The first geometry they proposed was a paraboloid.

On-axis beam perfectly focused (no spherical abberration), however, it is severely affected by Coma for off-axis sources.

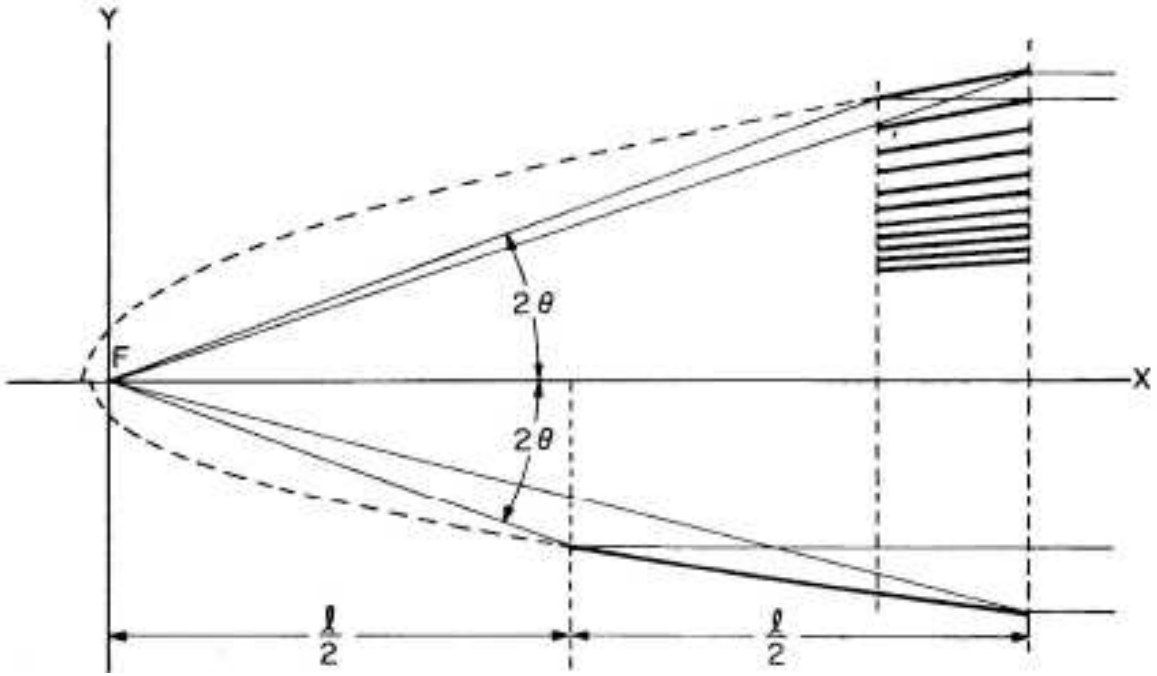

Ernst Abbe derived a condition that a focusing optical system has to approximately satisfy to be free of Coma abberration for off-axis sources and thus be able to form sharp images over a non negligible FOV. For a telescope focusing sources at large distance

Abbe Sine Condition

$$f = \frac{h}{\sin \vartheta}$$

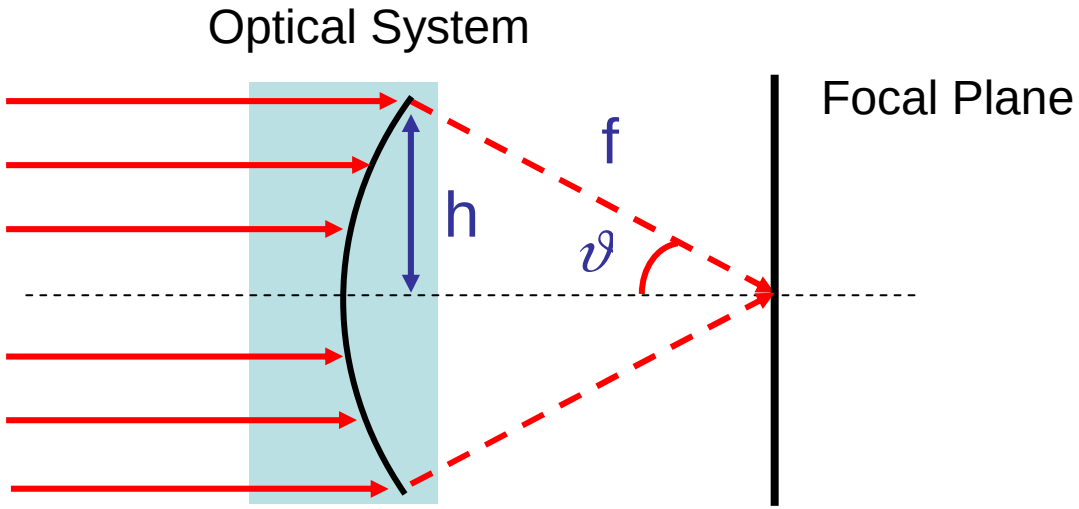

where θ is the angle between the incident and focused beams, h is the distance of the incident beam from the optical axis, and f is constant for all incident beams.

The Abbe Sine Condition is satisfied when the surface intercepting incident and focused beams is a sphere.

Two-Reflections Wolter Type

Hans Wolter demonstrated in 1952 that the reflection by a combination of two optical coaxial elements, a paraboloid and an hyperboloid, approximately satisfies the Abbe Sine Condition. He also demonstrated that the reflection by an even number of coaxial elements nearly satisfy the same condition.

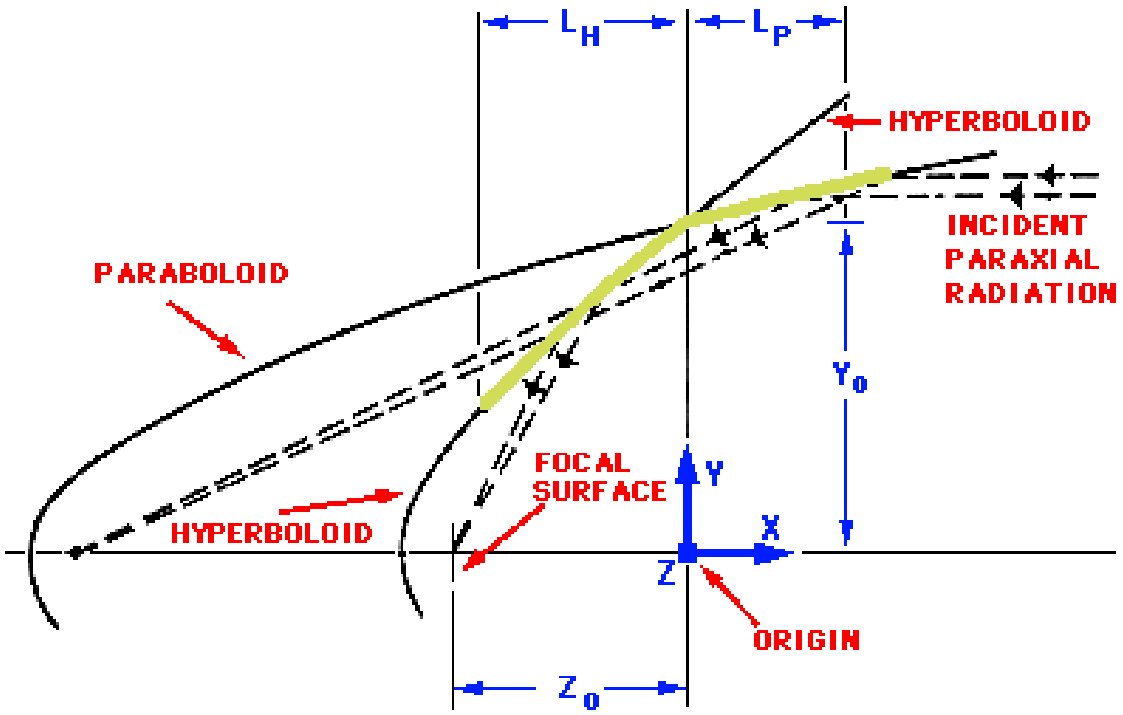

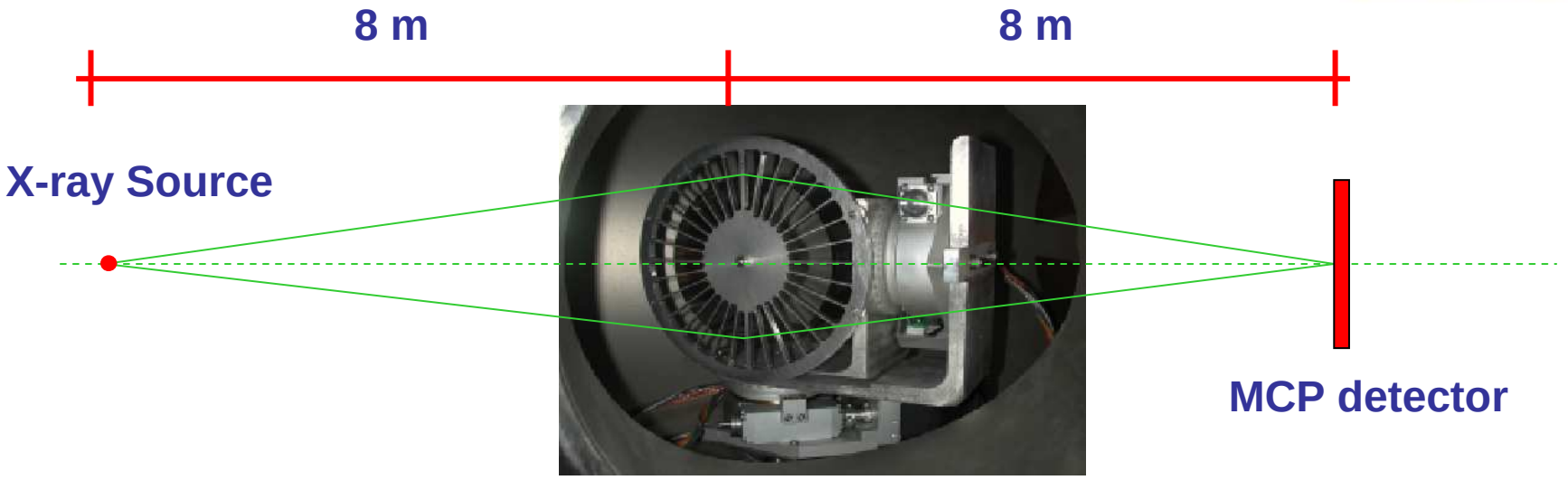

ON-AXIS

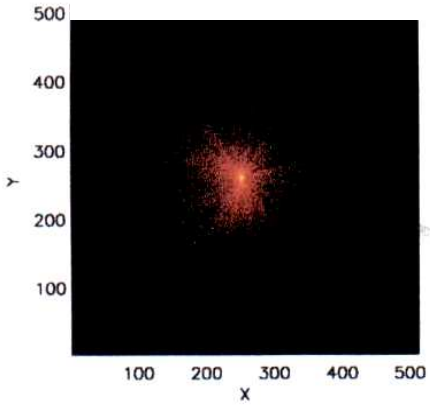

60" OFF-AXIS

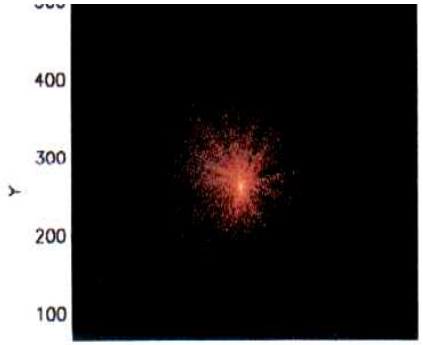

120" OFF-AXIS

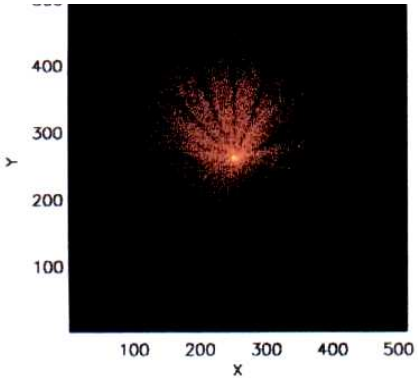

X-Ray image of a point source taken with a single reflection grazing incidence cilindrical optics (approximation of an ellipse) at the XACT facility of INAF-OAPA. Notice the strong Coma aberration of a single reflection optics.

Hans Wolter proposed three different configurations of a paraboloid and hyperboloid to focus X-Rays.

The Type I design is the most convenient among the three because:

1) Provides a better approximation of the Abbe Sine Condition

1) For the same effective area has the shortest focal length;

2) It allows to nest many shells to increase the collecting area.

Only the Type I design has been used for X-Ray Astronomy

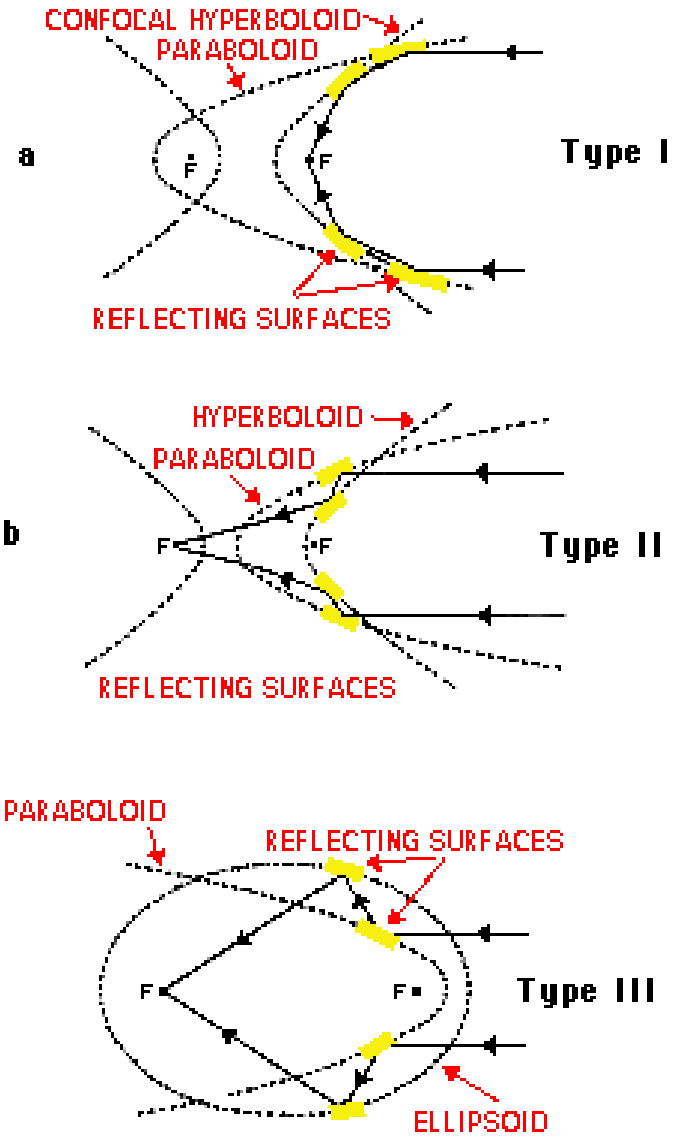

X-Ray Image of the Orion Nebula taken with the ROSAT PSPC. The ROSAT telescope is a Wolter type I. The Spherical aberration is the dominant effect that causes the images of a point source off-axis to be significantly larger than the image of a point source on-axis.

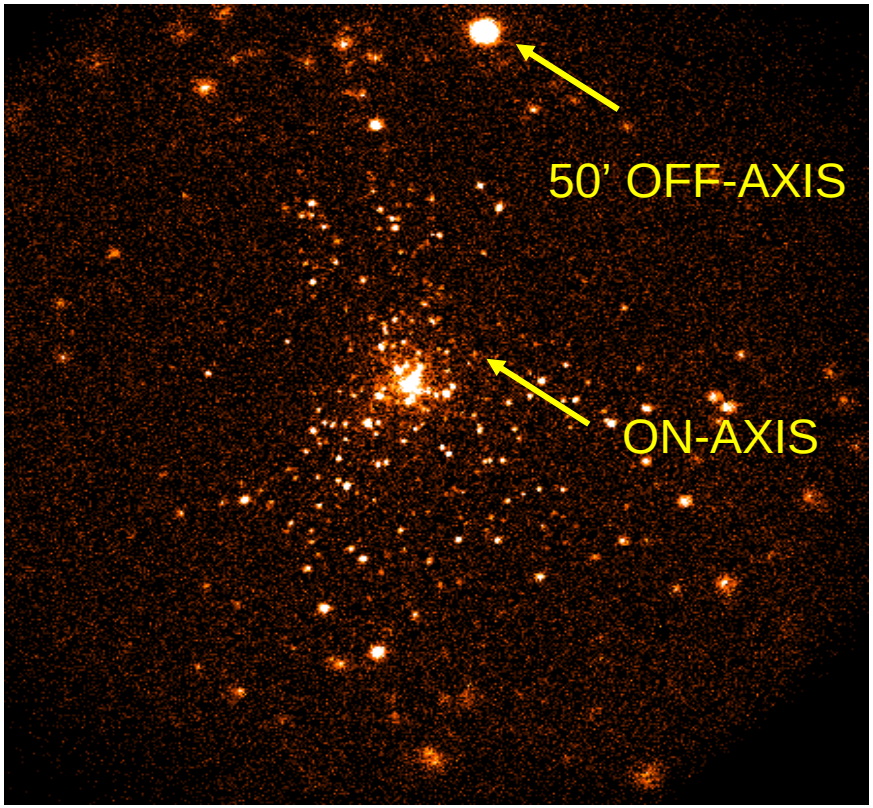

Spherical Aberration

Residual Coma

$$\sigma = 0.2 \frac{\tan^2 \gamma}{\tan \theta} \cdot \frac{L}{F} + 4 \tan \gamma \tan^2 \theta$$

σ = blur circle
θ = Angle of Incidence
γ = Off-Axis Angle
L = Mirror Height
F = Focal Length

Two-Cones Approx. to Wolter Type I

The paraboloid and hyperboloid sections of a Wolter type I optics can be approximated by two cones. When the intrinsic optical abberration of the telescope is non negligible, or the focal length is large and the height of the telescope is small the 2C approximation can be acceptable. The construction of cones is much simpler and less expensive than the construction of paraboloids or hyperboloids. The 2C approximation has been widely used in X-Ray Astronomy.

First image of the solar corona taken with a 2C optics in 1965 with a sounding rocket experiment.

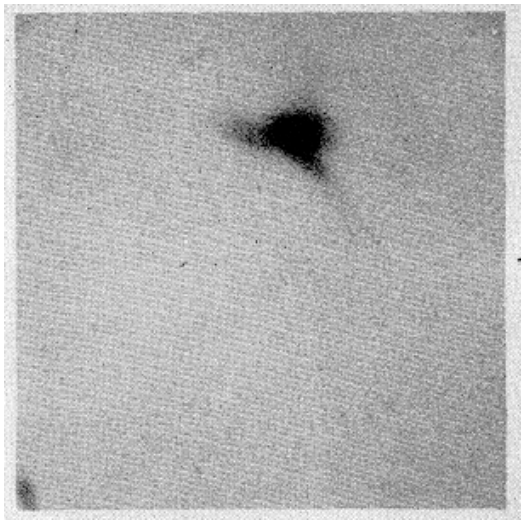

Giacconi et al. (1965), ApJ 142, 1274, "Solar X-Ray Images obtained using grazing Incidence Optics"

The Spiral Approximation to Two Cones

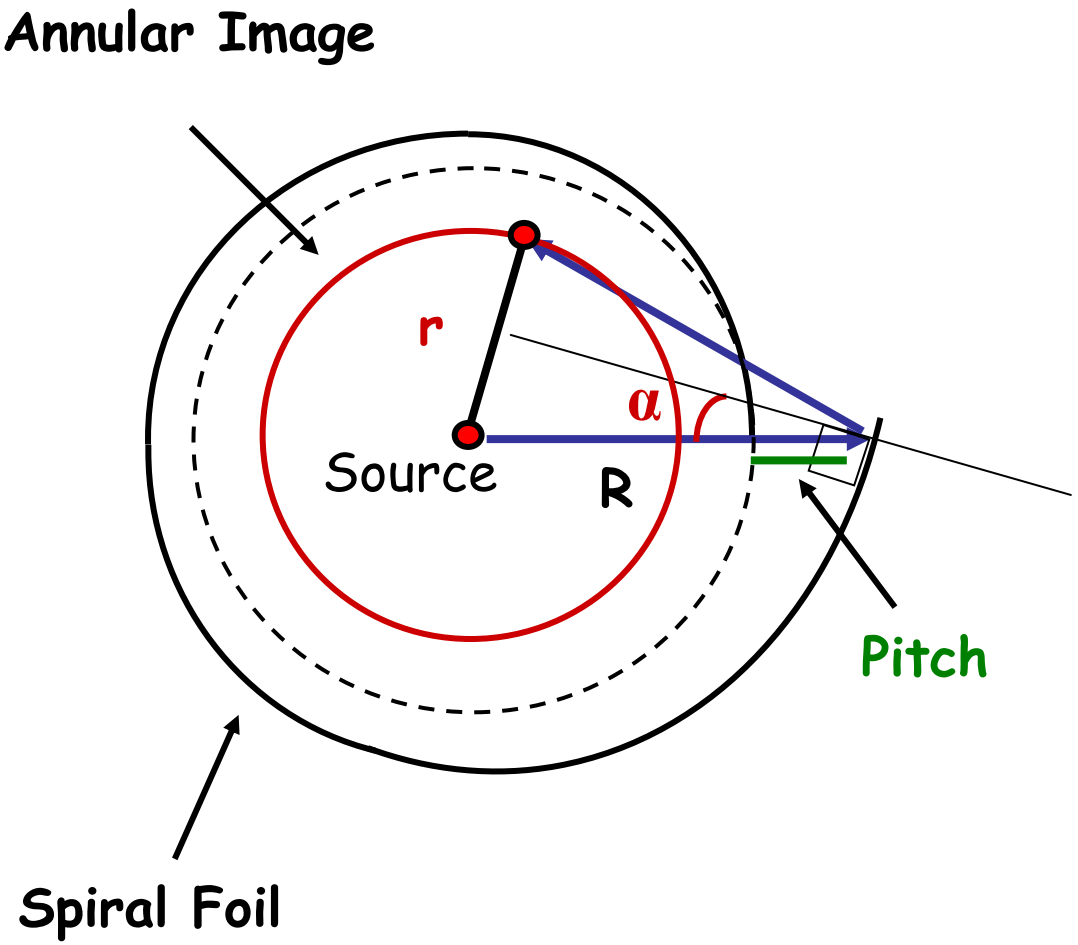

$$\alpha = \frac{\text{Pitch}}{2\pi R}$$

$$r \approx R \cdot 2\alpha$$

$$r \approx \frac{\text{Pitch}}{\pi}$$

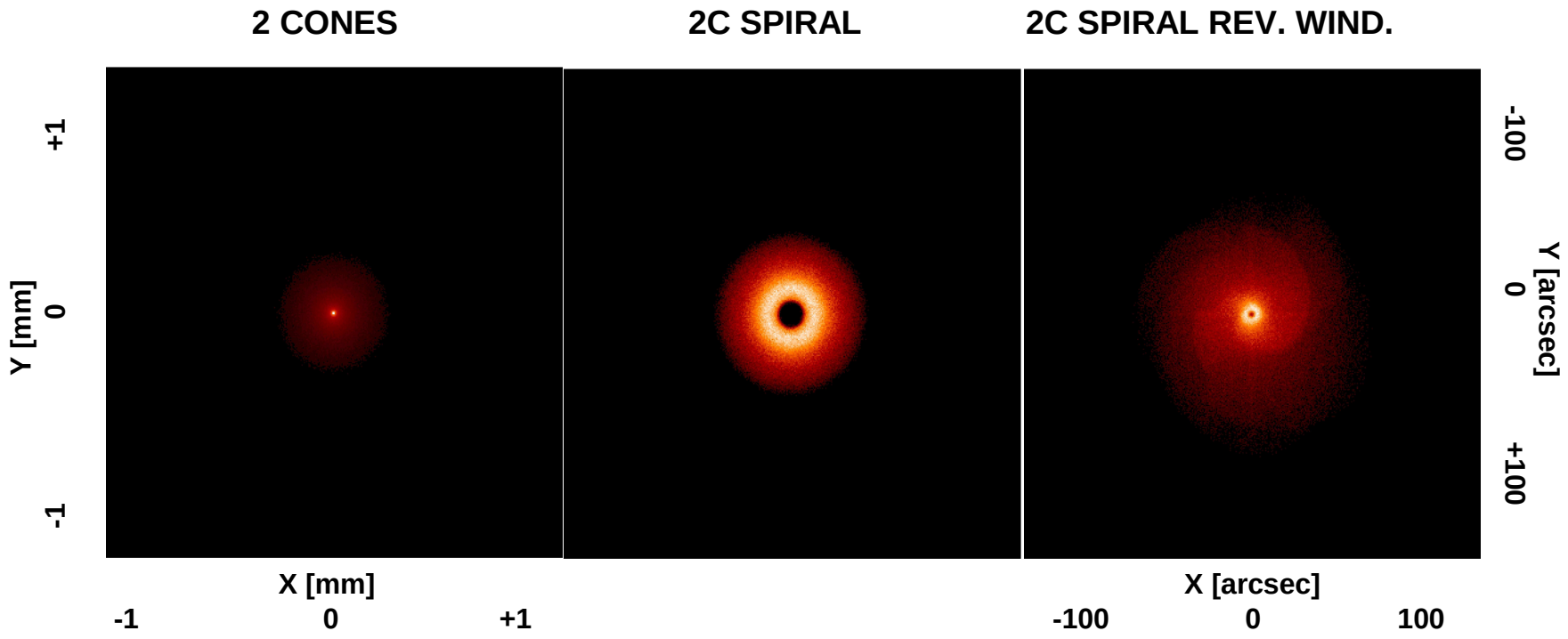

FL = 200.0 cm
O.R. = 10.0 cm
I.R. = 2.5 cm
Height = 10.cm

Ray Tracing Simulation provided by Teresa Mineo and Emanuele Perinati

Small Spiral Cylinder, Raytracing – 5' FWHM Scattering

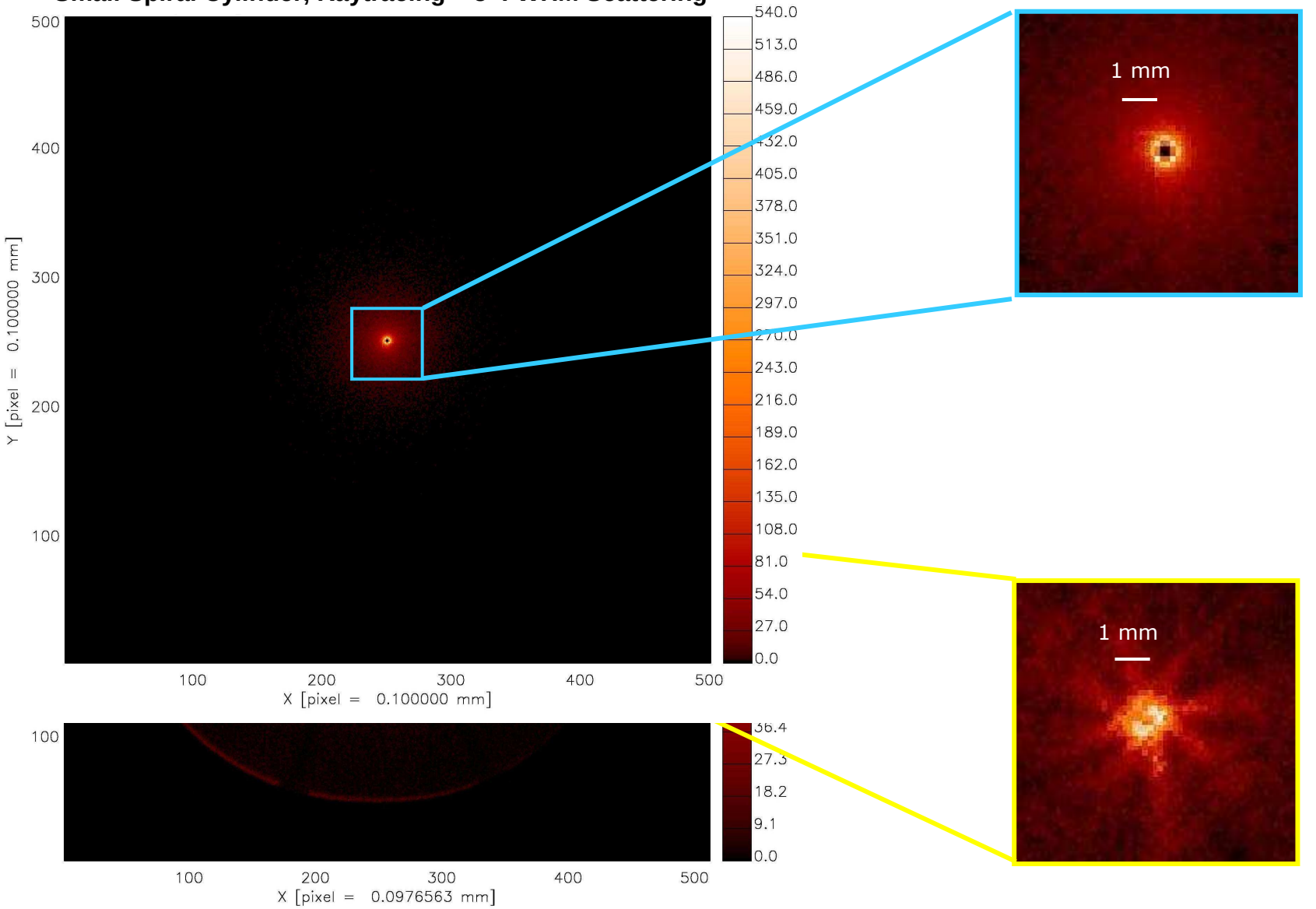

Other Approx. to Wolter Type I

Wolter-Schwarzschild design: it exactly satisfies the Abbe Sine Condition and it has been adopted for the Einstein mirrors; is coma free but it is strongly affected by spherical aberration (**Chase and VanSpeybroeck, (1972), Appl. Opt, 12, 1042**)

Polynomial Design: parameters are optimized to maintain the same HEW in a wide field of view. Introducing small aberration on-axis the off-axis imaging behavior is improved (**Burrows, Burg, and Giacconi, (1992), ApJ, 392, 760, and P. Conconi, S. Campana, (2001), A&A 372, 1088**).

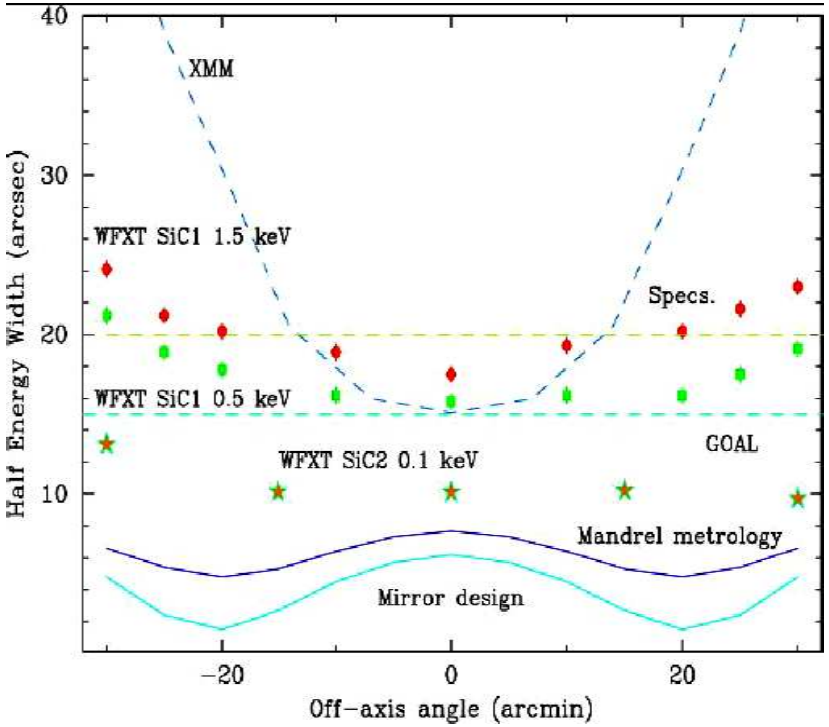

O. Citterio, et al., (1999), Proc. *SPIE,* 3766, 198.

Lobster Eye

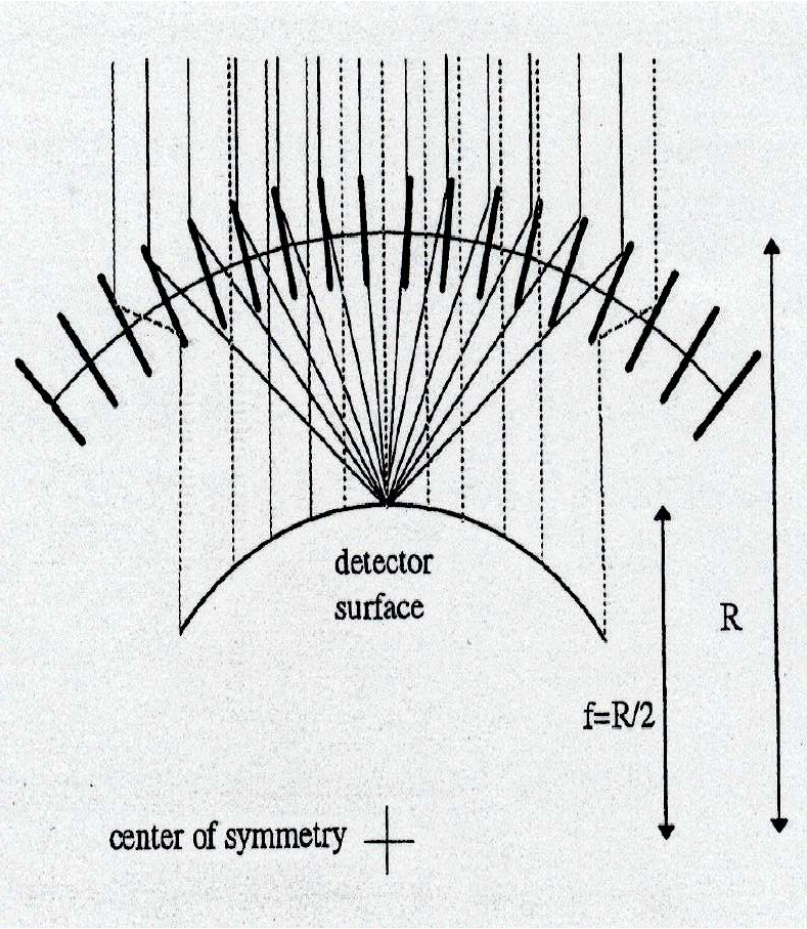

Designed to provide a very large FOV with a few arcmin angular resolution.

X-rays are focused to a line on the surface of a cylinder of radius R/2

Two such systems in sequence are necessary to provide 2D imaging

Construction Technologies

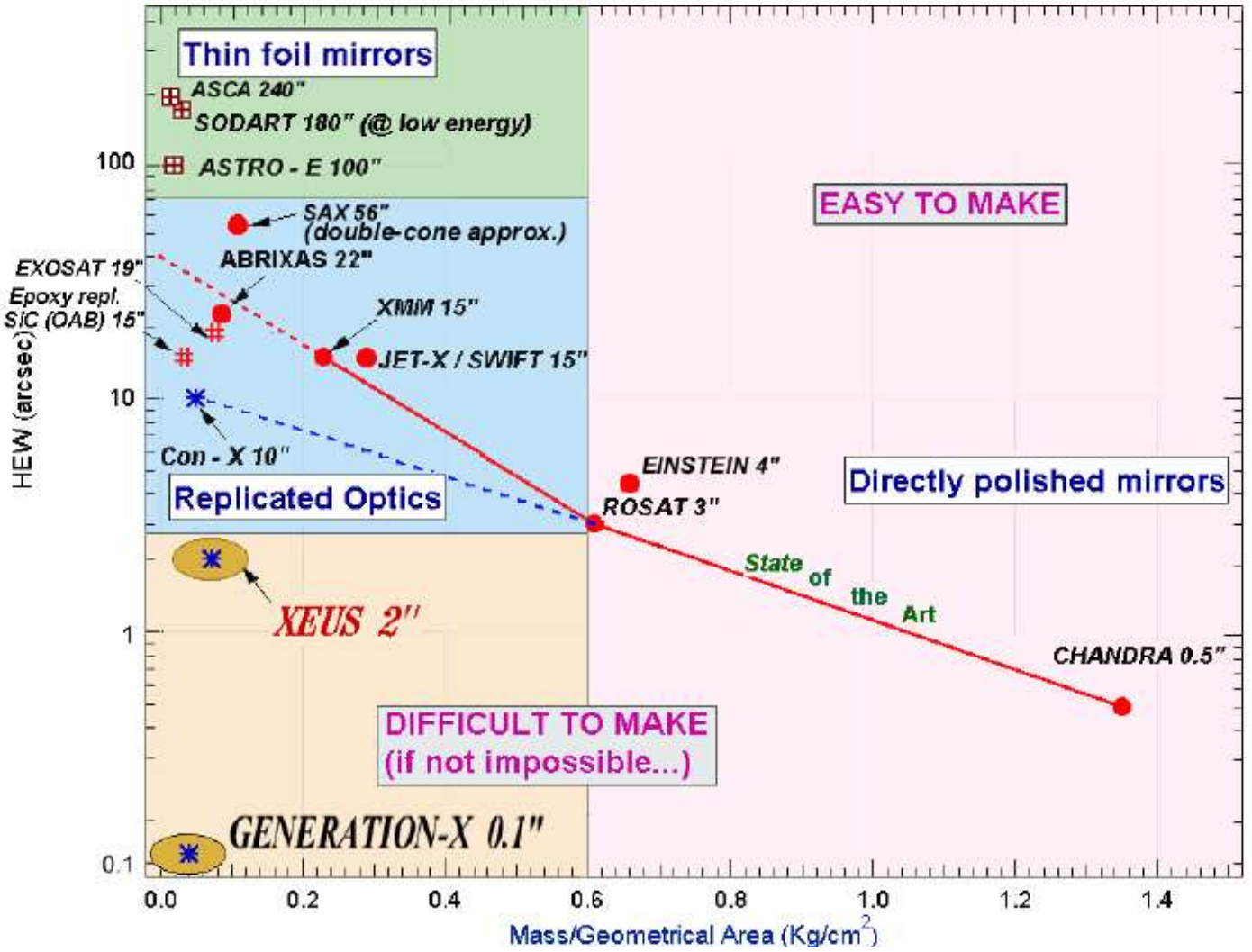

Citterio, et al., Proc. SPIE, 4496, 23 (2001)

Directly Polished Mirrors

Chandra High Resolution Mirror Assembly (HRMA)

Massive ceramic (e.g. Zerodur) mirror shells are directly formed starting from cylindrical shape by CNC machining, and precision grinding and optical polishing.

Projects: Einstein, Rosat, Chandra

Advantages: best achieved angular resolution

Drawbacks: high mirror walls and thus small number of nested mirror shells, high mass, extremely high cost process.

ROSAT

CHANDRA

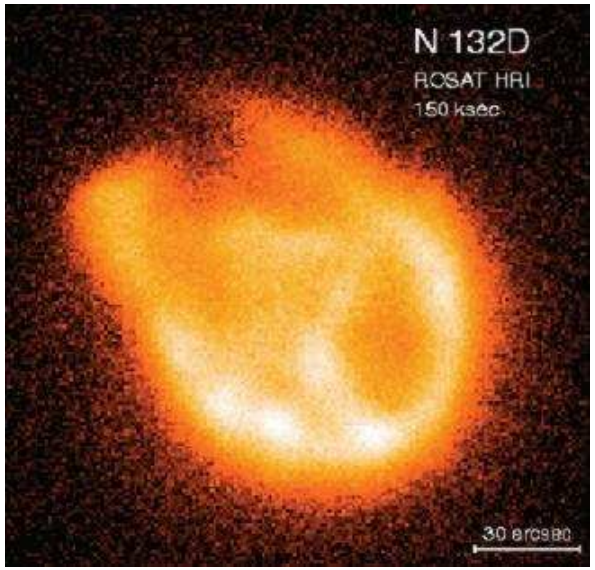

N132D a brigth SNR in LMC

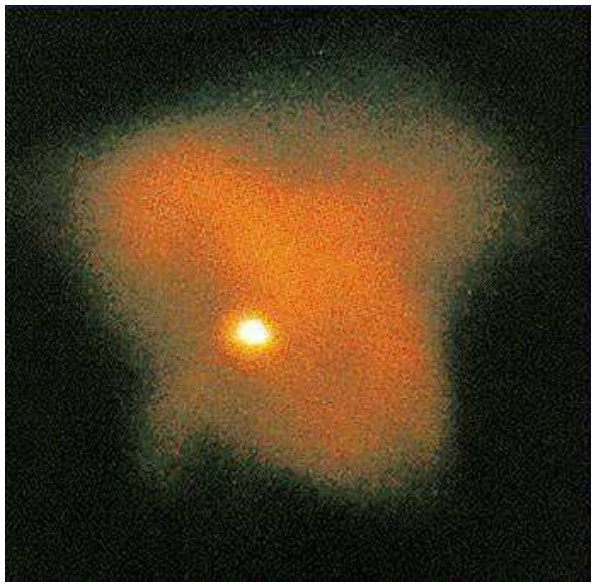

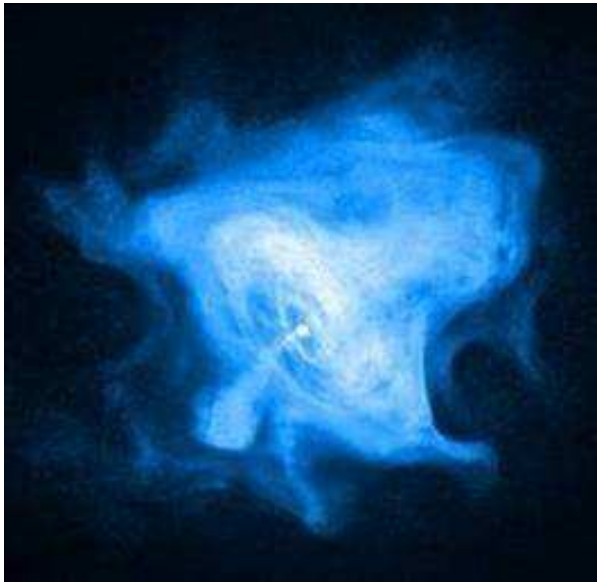

Crab Nebula

Replication

One of the three modules of the XMM-Newton Mirror Assembly

Mirror shells are built by electroforming or epoxy filling onto a super-polished mandrel. Detachment between shell and mandrel is obtained thermally by using the different thermal expansion coefficient of the two systems. Ni is the most used material for the shells altough SiC is also being explored to build ligther mirrors.

Projects: EXOSAT, SAX, JET-X/Swift, XMM

Advantages: good angular resolution, high mirror "nesting" the same mandrels for many modules

Drawbacks: relatively high cost process; high mass/geom. area ratio if Ni is used.

Thin Foils

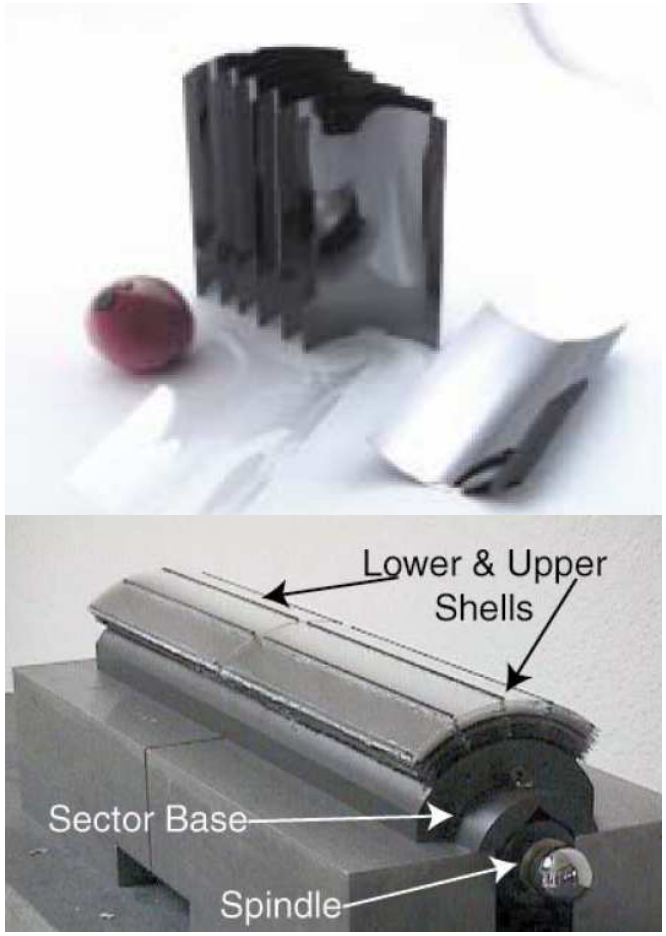

Thin foils assembly for the HEFT baloon born experiment.

Thin foil mirrors are obtained by thermally or mechanically forming flat sheets of Aluminum or Glass. A full revolution shell can be obtained by assemblying sectors.

Projects: ASCA, SODART, ASTRO-E, HEFT

Advantages: high mirror "nesting" possibility, low mass/geom. Area ratio, cheap process.

Drawbacks: until now low imaging resolutions (1-3 arcmin HEW)

Silicon Pore Optics

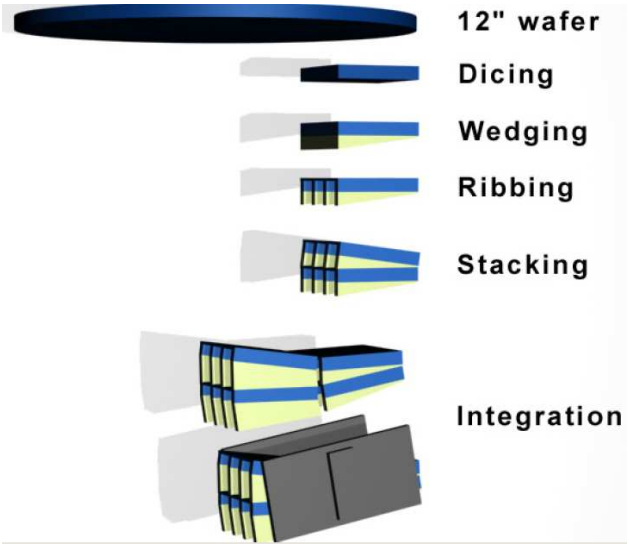

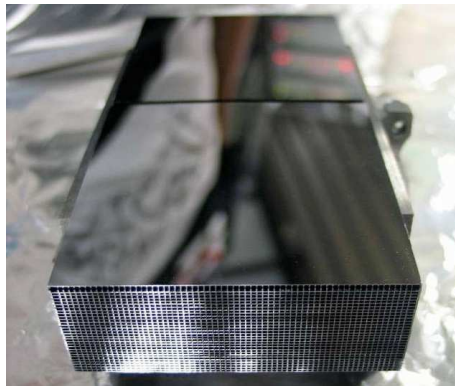

Basic idea and prototype developed by ESA and Cosine.

Silicon wafer polished on both sides with high surface quality are coated with a sacrificial SiO_2 layer that is wedged and groove machined. A large number of grooved wafers are stack into a module. Two modules are integrated to form a double reflection sector.

Projects: Investigated for XEUS (now IXO)

Advantages: high strength to weight mirror, rely upon wide industry experience on high quality wafer production, low mass/geom. Area ratio.

Drawbacks: Conical approximation to Wolter optics or K-B design (need long focal length and/or short height mirror). Many critical steps in the construction and integration procedures to be yet demonstrated.

Thin Plastic Foil Technology

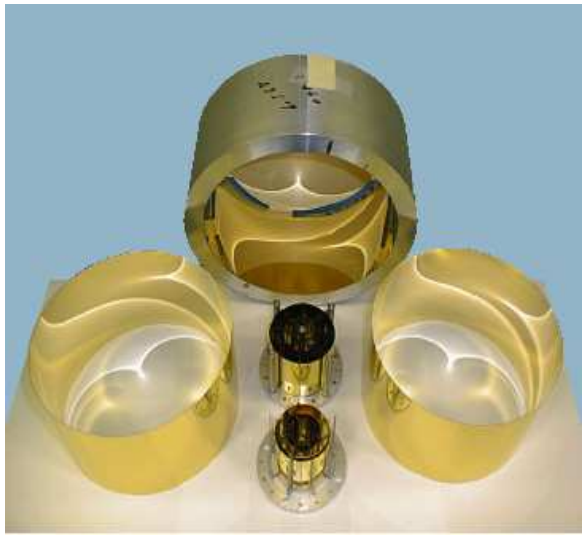

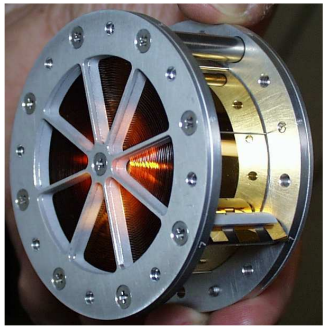

Thin Plastic Foils from industrial production lines with highly smooth surface quality is cut in long ribbons and shaped into full revolution surfaces (cilinders, cones).

Projects: R&D development

Advantages: No need for superpolished mandrels since mandrel provide only figure but not surface quality. Very low mass/geom. Area ratio. Very low cost. Allows construction of spiral approximation to conical optics.

Drawbacks: low imaging resolutions (1-5 arcmin HEW).

Schnopper et al. PROC. SPIE, 1999, 2001, 2002, 2004

Some References and Useful Tools

INTERNATIONAL ADVANCED SCHOOL
Leonardo da Vinci

"MISSION CONCEPT AND PAYLOAD DESIGN IN X- AND GAMMA-RAY ASTRONOMY"

Bologna, 1-12 July, 2002

http://www.iasfbo.inaf.it/events/ldavinci/programme/

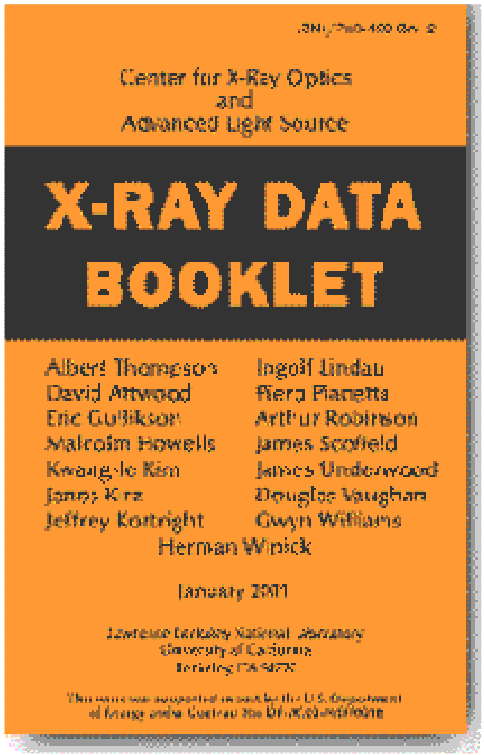

http://xdb.lbl.gov/

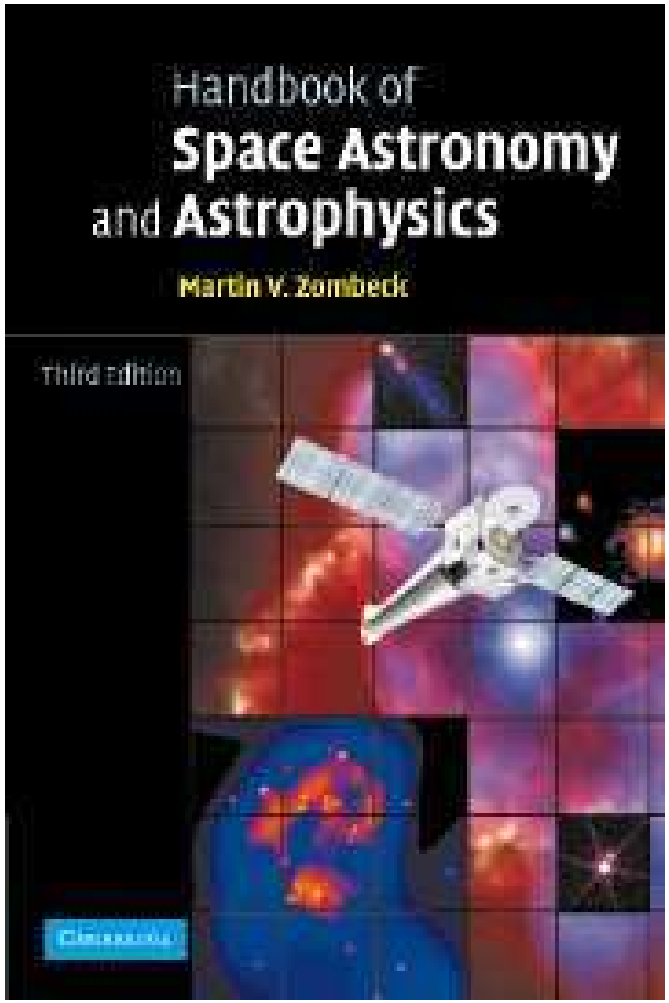

http://ads.harvard.edu/books/hsaa/

X-Ray Interactions With Matter

- Introduction
- Access the atomic scattering factor files.
- Look up x-ray properties of the elements.
- The index of refraction for a compound material.
- The x-ray attenuation length of a solid.
- X-ray transmission
  - Of a solid.
  - Of a gas.
- X-ray reflectivity
  - Of a thick mirror.
  - Of a single layer.
  - Of a bilayer.
  - Of a multilayer.
- The diffraction efficiency of a transmission grating.
- Related calculations:
  - Synchrotron bend magnet radiation.

Other x-ray web resources.

http://henke.lbl.gov/optical_constants/